Functional analysis of genetic variants in PALB2 and CHEK2: linking functional impact with cancer risk

Boonen, R.A.C.M.

CHAPTER 4

4

Functional analysis of genetic variants in the high-risk breast cancer susceptibility gene *PALB2*

Rick A.C.M. Boonen, Amélie Rodrigue, Chantal Stoepker, Wouter W. Wiegant, Bas Vroling, Milan Sharma, Magdalena B. Rother, Nandi Celosse, Maaike P.G. Vreeswijk, Fergus Couch, Jacques Simard, Peter Devilee, Jean-Yves Masson and Haico van Attikum

Published in *Nature Communications*
(PMID: 31757951)

ABSTRACT

Heterozygous carriers of germ-line loss-of-function variants in the DNA repair gene *PALB2* are at a highly increased lifetime risk for developing breast cancer. While truncating variants in *PALB2* are known to increase cancer risk, the interpretation of missense variants of uncertain significance (VUS) is in its infancy. Here we describe the development of a relatively fast and easy cDNA-based system for the semi high-throughput functional analysis of 48 VUS in human *PALB2*. By assessing the ability of *PALB2* VUS to rescue the DNA repair and checkpoint defects in *Palb2* knockout mouse embryonic stem (mES) cells, we identify various VUS in *PALB2* that impair its function. Three VUS in the coiled-coil domain of PALB2 abrogate the interaction with BRCA1, whereas several VUS in the WD40 domain dramatically reduce protein stability. Thus, our functional assays identify damaging VUS in *PALB2* that may increase cancer risk.

KEYWORDS

Breast Cancer; Variant of Uncertain Significance (VUS); PALB2; DNA Repair Homologous Recombination (HR); PARP inhibitor.

INTRODUCTION

Germline loss-of-function (LOF) variants in the breast cancer susceptibility genes *BRCA1* and *BRCA2* are known to result in an approximately tenfold increased lifetime risk of developing breast cancer (1). Similar to these genes, mono-allelic LOF variants in the gene encoding partner and localizer of *BRCA2* (*PALB2*) also increase the risk of breast cancer (2), whereas bi-allelic LOF variants cause Fanconi anemia (FA) (3). It is now well established that women who carry pathogenic variants in *PALB2* are at a similar risk for breast cancer as those who carry pathogenic variants in *BRCA2* (1,4). Therefore, *PALB2* takes a valid place on breast cancer predisposition gene panel tests and is becoming widely included in breast cancer clinical genetics practice. This has already led to the identification of numerous variants in *PALB2*, which may associate with breast cancer (as of September 2019, 1301 *PALB2* VUS have already been reported in ClinVar). However, current risk estimates for *PALB2* variants have so far only been based on truncating variants that are predicted to fully inactivate the protein (5). For most missense variants the impact on protein function is unclear and therefore the associated cancer risk is unknown. Assessment of pathogenicity of such variants of uncertain significance (VUS), therefore relies mostly on co-segregation with disease, co-occurrence with known pathogenic variants, and family history of cancer. To extend the utility of *PALB2* genetic test results, additional methods for interpreting VUS are urgently required.

A key facet of interpreting VUS in *PALB2* is understanding their impact on PALB2 protein function. PALB2 exists as oligomers that can form a complex with BRCA1 and BRCA2 and the recombinase RAD51 (6,7). This involves PALB2's N-terminal coiled-coiled domain for interaction with BRCA1 (7) and its C-terminal WD40 domain for interaction with BRCA2 (8). The PALB2-BRCA1/2-RAD51 complex plays an essential role in homologous recombination (HR), which is a critical pathway for the repair of highly-deleterious DNA double-strand breaks (DSBs). Following their detection, the ends of a DSB are resected to generate stretches of 3' single-stranded DNA (ssDNA), which are bound by the ssDNA-binding protein RPA. PALB2 becomes recruited to these resected DSB ends in a manner dependent on BRCA1 to facilitate the assembly of BRCA2 and RAD51 onto broken DNA ends. RAD51 in turn catalyzes strand invasion and DNA transfer, usually from a sister chromatid available in S/G2 phase (6,7,9), ultimately leading to error-free repair of DSBs.

Germline nonsense and frameshift variants in *BRCA1*, *BRCA2* and *PALB2* give rise to a characteristic genome instability signature that is associated with HR deficiency (10). Targeting this HR deficiency has proven to be effective in PARP inhibitor (PARPi)-based cancer treatment, during which the ensuing DSBs can be repaired by HR in healthy cells, but not in HR-deficient cancer cells (11,12). While PARP inhibitor-based therapy holds great promise for the treatment of HR-deficient cancers, a major obstacle is that clinical testing of

these tumors often reveals numerous VUS in *BRCA1*, *BRCA2* and *PALB2*, for which the effect on HR and the response to PARP inhibitor-based therapy is often unclear.

For *BRCA1* and *BRCA2*, functional assays that mostly use HR as a read-out have been established to assess the effect of VUS on protein function (13-17). These assays have successfully determined the functional consequences and potential therapy response of a variety of VUS. However, with regard to *PALB2*, the functional analysis of variants is still in its infancy even though there is a clear clinical demand. Here, we fill this gap by describing the development of a robust functional assay for the analysis of VUS in *PALB2*. The assay allows a semi high-throughput analysis of VUS in human *PALB2* cDNA in *Palb2* knockout mouse embryonic stem (mES) cells using HR, PARPi sensitivity and G2/M checkpoint maintenance as read-outs. We identify at least 14 *PALB2* VUS that strongly abrogate PALB2 function. Moreover, *PALB2* VUS located in the WD40 domain have a high tendency to impair PALB2 protein function by affecting its stability, whereas *PALB2* variants located in the coiled-coil domain tend to impair its interaction with BRCA1. Thus, we report on the development of a relatively rapid and easy functional assay that can determine the functional consequences of VUS in *PALB2*, thereby facilitating cancer risk assessment and predicting therapy response.

RESULTS

A cell-based functional assay for *PALB2* variants

For the analysis of *PALB2* variants we envisioned a cell-based assay that allows for reliable semi high-throughput testing of variants in human *PALB2*. This cell-based approach should combine efficient integration and equal expression of human *PALB2* cDNA carrying these variants in a cellular background devoid of endogenous *Palb2* and with the ability to assess their effect on HR. To this end, we introduced the well-established DR-GFP reporter into IB10 mES cells, which are highly proficient in HR (Fig.1a, Supplementary Fig. 1a-c) (18). The HR efficiency was nearly identical in all 3 correctly targeted clones (~10%) (Supplementary Fig. 1d) and clone 5 was selected for further experiments.

Next, we introduced the recombination-mediated cassette exchange (RMCE) system into cells from clone 5 (13). One component of this system, which consists of an acceptor cassette with F3 and Frt sites (Fig. 1a, Supplementary Fig. 2), was correctly integrated at the *Rosa26* locus in 1 out of 6 targeted clones (Supplementary Fig. 2a,b). The other component is an exchange cassette that carries a promoterless neomycin selection marker and an *EF1α* promotor fused to human *PALB2* cDNA flanked by F3 and Frt sites. This exchange cassette can be used for FlpO-mediated, site-specific integration of human *PALB2* cDNA at the RMCE acceptor cassette (Fig. 1a) (19). This would allow for stable expression of human *PALB2,*

which we envisioned in a cellular background devoid of endogenous *Palb2*.

Since knockout (KO) of *PALB2* is embryonic lethal (20-22), it has been notoriously difficult to generate *PALB2*^{KO} cells. However, since p53 deficiency could partially rescue *in utero* development of *Palb2*^{KO} mice, we decided to generate *Palb2*^{KO} mES cells in a p53-deficient background. In addition to facilitating the KO of *Palb2*, deficiency in both *p53 and Palb2* may also mimic tumor settings, as somatic *TP53* mutations are common in breast cancer associated with *BRCA1/2 (23,24)* and *PALB2 (25)*. We first employed CRISPR/Cas9-based genome editing to knockout mouse *Trp53* in cells harboring DR-GFP and the RMCE acceptor cassette (Fig. 1a,b, Supplementary Fig. 3a,b). Subsequent analysis of 4 *Trp53*^{KO} clones revealed that HR remained unaffected in these cells (Fig. 1b), allowing functional analysis in this genomic background using HR as a read-out. *Trp53*^{KO} clone-3 had the highest percentage of cells (~50%) with a normal chromosome number (*i.e*. 40 chromosomes) (Fig. 1c) and was therefore selected for further experiments.

Finally, we applied CRISPR/Cas9-mediated genome-editing to knockout mouse *Palb2* (Fig. 1d, Supplementary Fig. 3c,d). As expected, the efficiency of HR in the DR-GFP reporter assay was strongly reduced (by ~95%) in *Trp53*^{KO}/*Palb2*^{KO} cells when compared to that in *Trp53*^{KO} cells alone (Fig. 1d). To test whether human wild-type *PALB2* can complement this defect, we stably expressed wild-type human *PALB2* cDNA using RMCE (Fig. 1a). Importantly, due to site-specific integration, the promoterless neomycin gene will be driven by the endogenous *Rosa26* promoter, which enhances targeting efficiency and allows for selection of integrants on medium containing neomycin. Indeed, we observed *PALB2* expression in all individual neomycin resistant clones that were tested for *PALB2* expression (Supplementary Fig. 4a). However, since some differences in *PALB2* expression were observed between single clones, we pooled the neomycin-resistant clones (~500 clones) prior to examining the HR efficiency (Supplementary Fig. 4b), ruling out any effects on HR caused by differences in *PALB2* expression. We found that HR was efficiently rescued (by ~68%) following expression of human *PALB2* in the *Trp53*^{KO}/*Palb2*^{KO} cells compared to the *Trp53*^{KO} cells (Fig. 1d). Thus, we have developed a highly efficient cDNA-based complementation system for the functional analysis of variants in human *PALB2*.

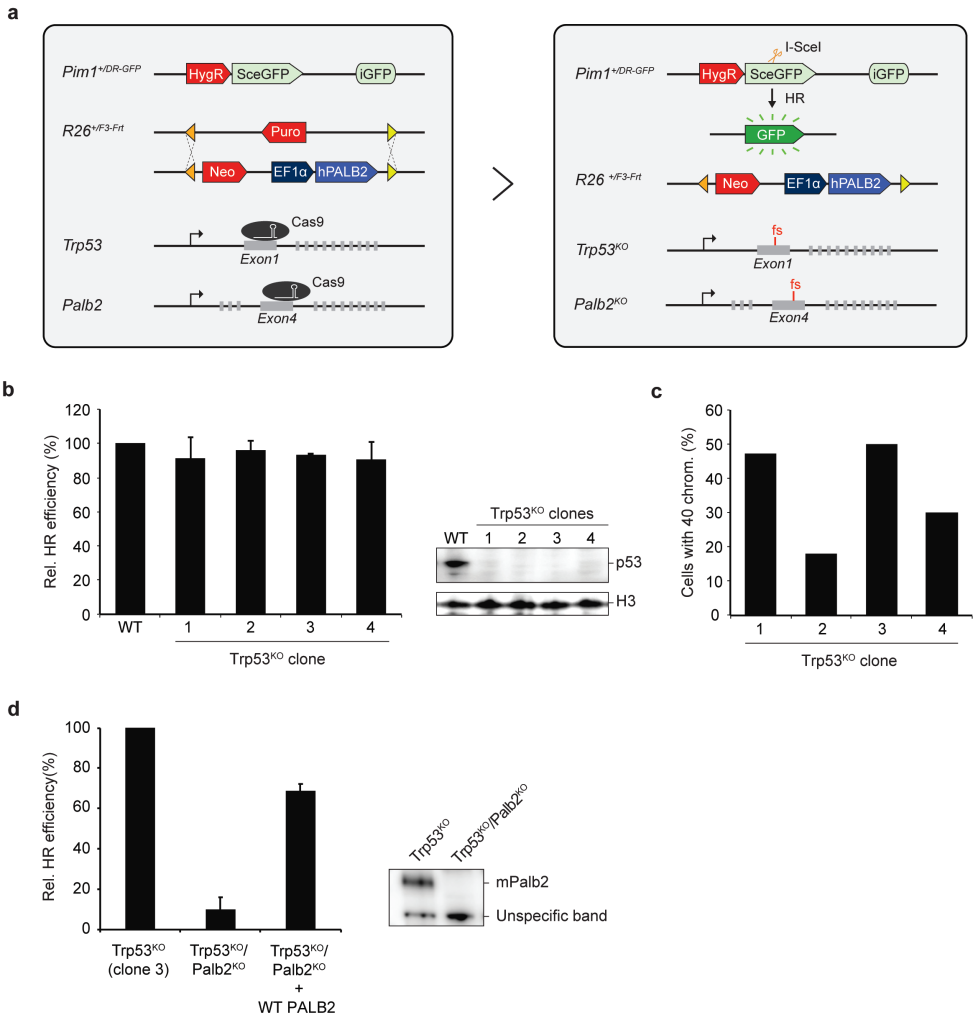

Figure 1. Development of a cDNA-based complementation system for the functional analysis of human *PALB2.* **a** Schematic of the cDNA-based complementation system for functional analysis of human *PALB2.* The DR-GFP reporter for HR and Recombination-Mediated Cassette Exchange system (RMCE) for site-specific integration and expression of a human *PALB2* cDNA were incorporated at the mouse *Pim1 and Rosa26* loci, respectively. Endogenous mouse *Trp53* was targeted with CRISPR/Cas with a gRNA for exon 1, whereas endogenous *Palb2* was targeted with a gRNA against exon 4 (left). Transient expression of the I-SceI endonuclease in *Trp53*^{KO}/*Palb2*^{KO} cells expressing human *PALB2* cDNA (with or without a variant) allows for assessment of the HR efficiency using the DR-GFP reporter (right). **b** DR-GFP assay in *Trp53*^{KO} mES cell clones co-transfected with I-SceI and mCherry expression vectors and GFP expression was monitored by FACS. Data represent mean percentages (± SEM) of GFP-positive cells among the mCherry-positive cells relative to that for the wild type (WT), which was set to 100%, from 2 independent experiments (left). Western blot analysis of *Trp53* expression in *Trp53*^{KO} 4 mES cell clones. Histone 3 (H3) was a loading control (right). **c** Karyotyping of *Trp53*^{KO} mES clones from **b**. The bar graph shows the percentages of cells with 40 chromosomes (n = 50 cells per condition). **d** DR-GFP assay in *Trp53*^{KO} and *Trp53*^{KO}/*Palb2*^{KO} mES cells expressing wild-type *PALB2* or

not. Cells were co-transfected with I-SceI and mCherry expression vectors and GFP expression was monitored by FACS. Data represent mean percentages (± SEM) of GFP-positive cells among the mCherry-positive cells relative to that for *Trp53*^{KO} cells, which was set to 100%, from 4 independent experiments (left). Western blot analysis of Palb2 expression in *Trp53*^{KO} and *Trp53*^{KO}/*Palb2*^{KO} (clone 3) mES cells (right). An unspecific band was a loading control (right). Source data are provided as a Source Data file.

Validation of a cell-based functional assay for *PALB2* variants

To evaluate our system, we selected 12 truncating *PALB2* variants (Fig. 2a, *red*) that are known to be deleterious and associate with cancer and/or Fanconi anemia (3,4,26-28). In addition, we selected 8 missense variants from the dbSNP database (Fig. 2a, *green*), which we expect to be benign/neutral because of their frequency in the general population (between 0.1-15% based on the 1000 Genomes Project). Site-directed mutagenesis was used to introduce these variants, as well as a synonymous variant (c.2574T>C, p.V858=), into the RMCE vector that carries human *PALB2* cDNA. Sequence-verified constructs were introduced by RMCE into the *Trp53*^{KO}/*Palb2*^{KO} mES cells, which were then subjected to DR-GFP assays. As expected, HR was dramatically reduced in cells carrying the empty vector (Ev) when compared to cells expressing human *PALB2* cDNA (*i.e.* reduction in HR of ~90-95%) (Fig. 2b). Similarly, cells expressing human *PALB2* with a truncating variant displayed strong defects in HR. In contrast, cells that expressed either the benign/neutral variants or the synonymous variant showed HR levels comparable to that of cells expressing wild-type *PALB2* (Fig. 2b).

To corroborate these findings, we also examined whether cells expressing benign/neutral or truncating *PALB2* variants display sensitivity to PARPi. As expected, we found that *Trp53*^{KO}/*Palb2*^{KO} cells complemented with the Ev were hypersensitive to PARPi when compared to those expressing wild-type human *PALB2* cDNA (Fig. 3a, Supplementary Figs. 5, 6 and 7). Moreover, the expression of truncating *PALB2* variants led to a dramatically increased sensitivity to PARPi (at least by ~70%), while that of the benign/neutral variants did not (Fig. 3a, Supplementary Fig. 5). Thus, by measuring HR efficiencies using DR-GFP and PARPi sensitivity, our cell-based system reproducibly classifies benign/neutral and pathogenic/truncating variants based on their effect on PALB2 function in HR.

Functional analysis of *PALB2* VUS

In contrast to truncating variants in *PALB2*, the contribution of missense variants with respect to cancer risk is largely unclear. We therefore analyzed the effect of 48 *PALB2* VUS and one synthetic missense variant (p.A1025R) (Fig. 2a, *blue*) (29). Many of these VUS have been identified during a multigene panel analysis for a large case-control association study performed by the BRIDGES consortium. In addition, several VUS were gathered from ClinVar (p.I944N, p.L24S and p.L1070P) and literature (p.K18R, p.Y28C, p.L35P, p.R37H) (30,31).

Interestingly, we observed strong HR defects in DR-GFP assays for p.L35P-, p.W912G-, p.I944N-, p.L961P-, p.G1043D-PALB2, exhibiting a ~90-95% reduction in HR, comparable to the truncating *PALB2* variants and the empty vector conditions (Fig. 2b). In addition, we also observed strong effects on HR for several other VUS (p.L24S, p.Y28C, p.G937R, p.L947S, p.L972Q, p.T1030I, p.I1037T, p.L1070P, p.L1172P), as well as the synthetic missense variant p.A1025R in PALB2, reducing HR by ~60-90% when compared to wild-type PALB2 (Fig. 2b). A FACS-based cell cycle analysis for 33 selected *PALB2* variants showed no effect on cell cycle distribution (Supplementary Fig. 8), excluding the possibility that effects on HR were due to differences in cell-cycle progression.

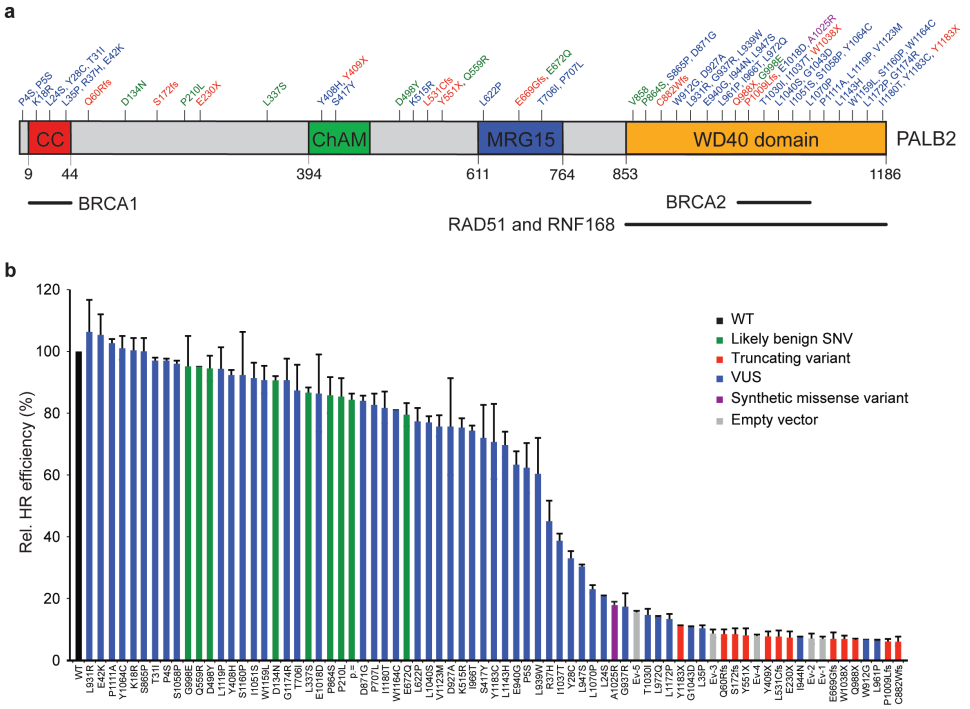

Figure 2. Human *PALB2* variants and their effect on HR. **a** Schematic representation of the PALB2 protein with variant positions indicated and categorized as either neutral (green), truncating (red), VUS (blue) and synthetic missense variant (purple). The amino acid numbers are shown to specify the evolutionarily conserved functional domains of PALB2. PALB2 regions involved in the interactions with BRCA1, BRCA2, RNF168 and RAD51 are indicated. **b** DR-GFP assay in *Trp53*^{KO}/*Palb2*^{KO} mES cells expressing human *PALB2* variants (or an empty vector control, Ev). Cells were co-transfected with I-SceI and mCherry expression vectors and GFP expression was monitored by FACS. Data represent mean percentages (± SEM) of GFP-positive cells among the mCherry-positive cells relative to wild type (WT), which was set to 100%, from 2 independent experiments, except for p.L939W and p.G998E for which data from 3 independent experiments are presented. Variants/conditions are categorized by color

as either wild type (WT, black), likely benign SNV (green), truncating variant (red), VUS (blue), synthetic missense variant (purple) or empty vector (Ev, grey). Ev1-5 refer to Ev controls from 5 different replicates. Source data are provided as a Source Data file.

Next, we examined the effect of the 48 selected VUS and p.A1025R on PARPi sensitivity using a cellular proliferation assay. We observed that 11 VUS (p.Y28C, p.L35P, p.W912G, p.G937R, p.I944N, p.L947S, p.L961P, p.L972Q, p.T1030I, p.G1043D and p.L1172P), as well as p.A1025R, displayed sensitivity to PARPi treatment comparable to that observed for *PALB2* truncating variants (Fig. 3a, Supplementary Fig. 6,7). Importantly, when comparing the HR efficiency measured by DR-GFP and PARPi sensitivity assays, a strong positive correlation was observed for all variants tested (R^2*=0.804*) (Fig. 3b). These results indicate that our complementary cell-based assays can determine the functional consequences of VUS in human *PALB2*. Most notably, taking the data from both assays into account, we identified at least 5 VUS (p.L35P, p.W912G, p.L961P, p.I944N and p.G1043D) that affect PALB2 function to a similar extent as the truncating variants. The effect of these VUS on PARPi sensitivity was further evaluated using a clonogenic survival assay. This revealed that 4 *PALB2* VUS (p.W912G, p.L961P, p.I944N and p.G1043D) also render cells hypersensitive to prolonged treatment with lower concentrations of PARPi (Fig. 3c). Consequently, such VUS may confer an increased cancer risk and serve as a target for PARPi-based therapy.

While PARPi treatment holds great promise for the treatment of HR-deficient tumors, an alternative strategy may be to treat with interstrand crosslink (ICL)-inducing chemotherapeutic drugs, since ICLs require HR for their repair (32). We therefore analyzed several *PALB2* variants in their response to the ICL-inducing agent cisplatin. As expected, two truncating variants p.Y551X and p.Y1183X displayed strong sensitivity to cisplatin comparable to the empty vector condition (Fig. 3d). Consistent with the effects observed in the HR and PARPi assays, three PALB2 VUS (p.L35P, p.L961P and p.G1043D) were also sensitive to cisplatin. When comparing the HR efficiency measured by DR-GFP to cisplatin sensitivity, a strong correlation (R^2*=0.8313)* was observed (Fig. 3e). Thus, VUS in *PALB2* that impair HR may serve as targets for both PARPi- and ICL-based chemotherapy.

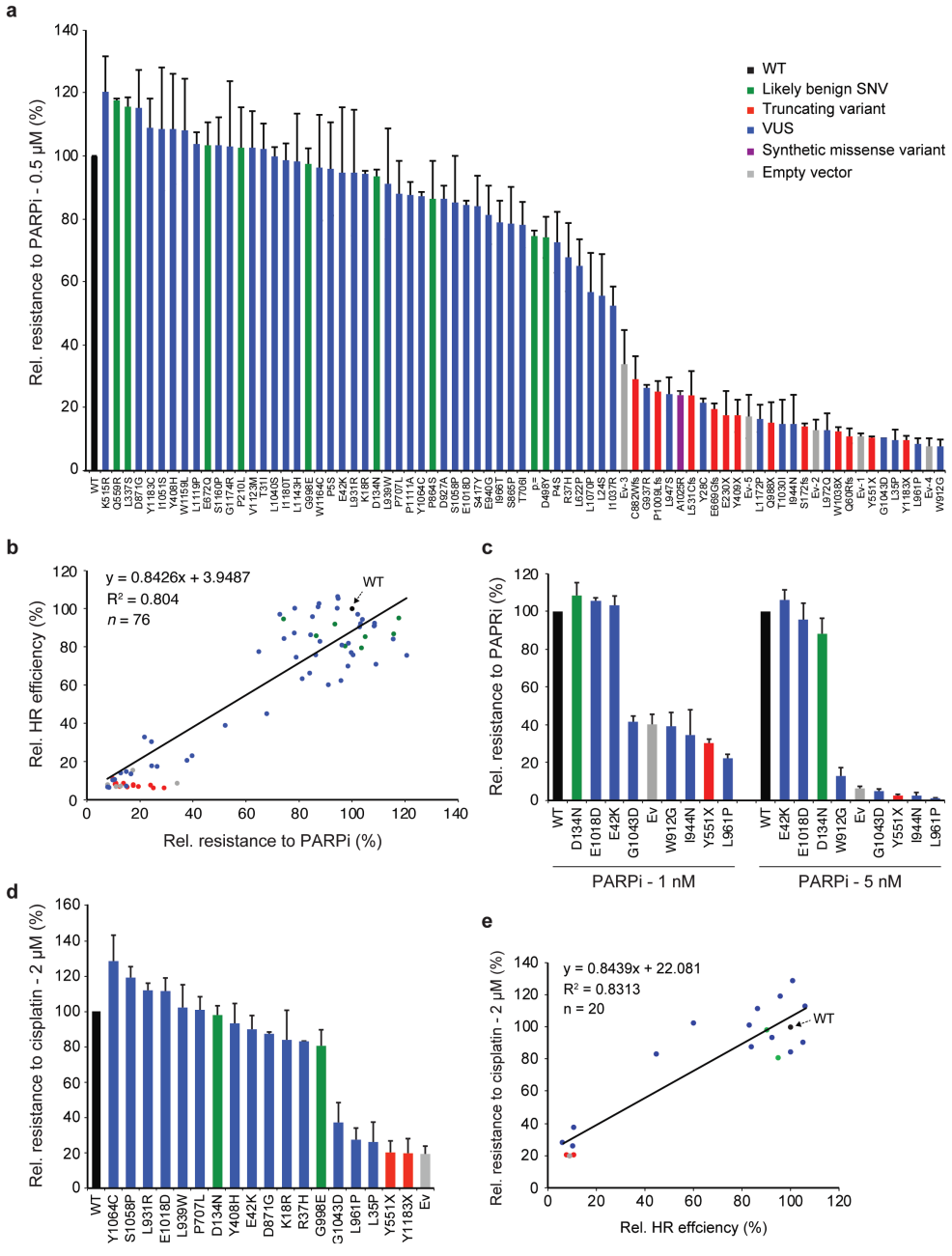

Figure 3. Functional analysis of *PALB2* VUS using PARP inhibitor and cisplatin sensitivity assays. **a** Proliferation-based PARP inhibitor (PARPi) sensitivity assay using *Trp53*^{KO}/*Palb2*^{KO} mES cells expressing human *PALB2* variants (or an empty vector control, Ev). Cells were exposed to 0.5 µM PARPi for two days. Cell viability was measured 1 day later using FACS. Data represent the mean percentage of viability relative to wild type (± SEM), which was set to 100%, from 2 independent

experiments, except for p.P4S, p.P210L, p.L939W and p.V1123M, for which data from three independent experiments is presented, and p.L24S, p.L1070P for which data from four independent experiments is presented. Variants/conditions are categorized by color. **b** Scatter plot showing the correlation between HR efficiencies and PARPi sensitivity measured in Fig. 2a and **b**, respectively. Variants/conditions are categorized by color as in **a**. The trendline indicates the positive correlation between the outcome of DR-GFP and PARPi sensitivity assays. **c** Clonogenic PARP inhibitor survival assay using *Trp53*^{KO}*/Palb2*^{KO} mES cells expressing human *PALB2* variants (or an empty vector control, Ev). Cells were exposed to the indicated concentrations of PARPi for 7-9 days after which surviving colonies were counted. Data represent the mean percentage of survival (± SEM) relative to cells expressing wild-type *PALB2*, which were set to 100%, from 3 independent experiments upon in case of treatment with 1 nM PARPi, and 4 experiments in case of treatment with 5 nM PARPi. Variants/conditions are categorized by color as in **a**. **d** As in **a**, except that cells were exposed to 2 μM cisplatin. Data represent the mean percentage of viability relative to wild type (± SEM), which was set to 100%, from 2 independent experiments. **e** Scatter plot showing the correlation between HR efficiencies and cisplatin sensitivity measured in Fig. 2b and **d**. The trendline indicates the positive correlation between the outcome of DR-GFP and cisplatin sensitivity assays. Variants/conditions are categorized by color as in **a**. Source data are provided as a Source Data file.

Correlation of functional analysis and *in silico* prediction

We next compared the outcome of our functional assays with the predictions of several *in silico* algorithms for all missense variants. For the prediction tools that give categorical results for missense variants, including PolyPhen (33), SIFT (34), and AlignGVGD (35), we observed little to no correlation with the outcome of DR-GFP and PARPi sensitivity assays (Supplementary Data 1). For instance, if we assume an HR efficiency of 40% or lower as damaging in the DR-GFP assay, then 24.1% of the missense variants (likely benign and VUS) are classified as damaging in our functional assay. However, we observed a gross overrepresentation of damaging variants when using PolyPhen (86.2%), SIFT (77.6%) and AlignGVGD (36.2%, counting C55 and C65). With respect to the latter, extreme caution should be taken as AlignGVGD classified at least two variants, which we found to be similarly damaging as truncating variants, as likely benign (p.W912G (C0) and p.I944N (C15); Supplementary Data 1). For *in silico* prediction tools that assign a continuous prediction score, such as (CADD (36) and REVEL (37)), we similarly observed a poor correlation with the outcome of DR-GFP and PARPi sensitivity assays (Supplementary Fig. 9). For instance, based on cut-offs of 0.0-0.5 for benign variants and 0.5-1.0 for damaging variants, REVEL would only categorize three of the PALB2 VUS (p.D871G, p.W912G and p.L931R) as damaging. However, both p.D871G and p.L931R appear to be fully functional in our assays. Thus, while REVEL severely underestimates the effects of VUS on protein function, it may also lead to false-positive predictions. Based on these observations, we conclude that predictive algorithms, as opposed to our functional analysis, are poor in predicting the effect of VUS on PALB2 protein function.

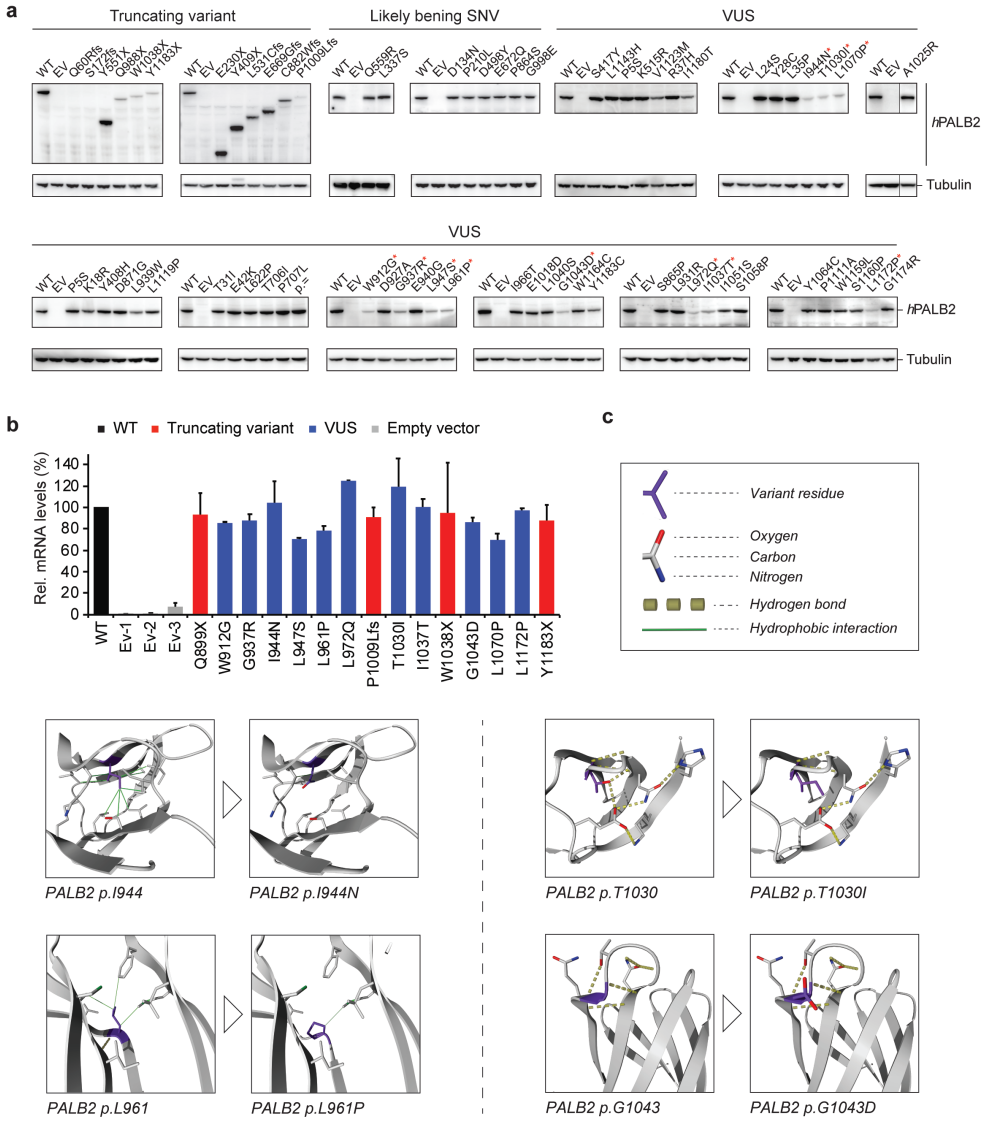

Figure 4. Effect of *PALB2* variants on protein expression and/or stability. **a** Western blot analysis of the expression of human *PALB2* variants in *Trp53*^{KO}/*Palb2*^{KO} mES cells using an antibody directed against the N-terminus of PALB2. Wild-type (WT) human PALB2 and empty vector (Ev) served as controls on each blot. Tubulin was used as a loading control. Marked PALB2 variants (red *) showed low levels of protein expression. **b** RT-qPCR analysis of human *PALB2* variants from A with low expression levels (red *). Primers specific for human *PALB2* cDNA and the *Pim1* control locus were used. Data represent the mean percentage (± SEM) of *PALB2* mRNA relative to wild type, which was set to 100%, from 2 independent RNA isolation experiments. Variants/conditions are categorized by color as either wild type (WT, black), truncating variant (red), VUS (blue) or empty vector (Ev, grey). Ev-1, -2, -3 refer to Ev controls from 3 different replicates. **c** Partial structures of the PALB2 WD40 domain showing the effect of 4 PALB2 variants exhibiting low protein expression as shown in **a**. Partial structures without and with

variant are shown side by side for each variant, indicating loss of stabilizing interactions (but not any possible conformational changes). Source data are provided as a Source Data file.

VUS in the PALB2 WD40 domain affect protein stability

Having identified *PALB2* variants that affect HR, we sought to address their mechanism of action. To this end, we first examined their effect on PALB2 expression by western blot analysis. For all benign variants, PALB2 expression was comparable to that of wild-type PALB2 (Fig. 4a). Similarly, most truncating and missense variants were unaffected in their expression levels, although the truncating variants resulted in the expression of the expected smaller proteins. However, for some truncating variants (p.Q899X, p.P1009Lfs, p.W1038X and p.Y1183X) and VUS located in the C-terminal WD40 domain (p.W912G, p.G937R, p.I944N, p.L947S, p.L961P, p.L972Q, p.T1030I, p.I1037T, p.G1043D, p.L1070P, p.L1172P), low levels of expression were observed (Fig. 4a, *red asterisk*). Reverse transcription-quantitative (RT-q)PCR analysis indicated that these variants did not affect expression at the mRNA level (Fig. 4b). This suggests that the low abundance of PALB2 protein is likely the result of protein misfolding and/or instability.

Crystal structure studies of the PALB2 C-terminal WD40 domain suggested that loss of the last 3 amino acids of PALB2 caused by the FA-associated p.Y1183X variant disrupts the hydrogen bonding in the seventh blade of the WD40 domain (3,29). Consistently, we also observed strongly reduced expression of PALB2 carrying this variant (p.Y1183X) (Fig. 4a). Thus, p.Y1183X may lead to in an incompletely folded PALB2 protein that is likely to be degraded rapidly. As such, it is not surprising that other truncating variants in the WD40 domain result in expression of a truncated protein that is unstable and degraded quickly. However, truncating PALB2 variants that lack the entire WD40 domain (p.E230X, p.Y409X, p.L531Cfs, p.Y551X, p.E669Gfs) appeared to express well (Figs. 2a and 4a). Nevertheless, they have likely lost all of their ability to interact with BRCA2 and RAD51, thereby impairing HR completely. Consistently, we observed almost no difference in the extent to which the different truncated forms of PALB2 affect HR.

Our results suggest that the WD40 domain of PALB2 is extremely sensitive to variants that affect protein folding and/or stability. Using the crystal structure of the WD40 domain (2W18) (29), *in silico* modeling of all PALB2 VUS that display low expression levels indeed showed that all these amino acid substitutions are extremely unfavorable for correct folding of this domain. Starting with p.I944N, we see that this isoleucine is a well-conserved hydrophobic residue that is located in an antiparallel β-sheet and whose side-chain is part of a tightly packed hydrophobic environment (Fig. 4c). Replacement of this isoleucine with an asparagine will lead to the loss of stabilizing hydrophobic interactions due to the energetically unfavorable presence

of a hydrophilic residue in a very hydrophobic environment. These opposed effects may destabilize the local environment and/or lead to folding problems. Comparable effects are predicted for p.L947S, p.L972Q and p.I1037T (Supplementary Fig. 10). L961 is another example of a residue that is located in a β-sheet and is involved in several hydrophobic interactions (Fig. 4c). When it changes into a proline (p.L961P), all of these local interactions are lost. Furthermore, proline is unfavored, because it results in the loss of a backbone hydrogen bond, thereby destabilizing the β-sheet. Comparable effects are predicted for p.W912G, p.L1070P and p.L1172P (Supplementary Fig. 10). However, for p.W912G the change into a very small glycine is also thought to result in excess flexibility at a position where this is not desired.

The side-chain of the hydrophilic residue p.T1030 is involved in an extensive network of hydrogen bonds and electrostatic interactions that extends across all 4 strands of the β-sheet (Fig. 4c). This variant will impair the formation of hydrogen bonds as isoleucine is not capable of these bonds through its sidechain. Consistent with our findings (Fig. 4a), an earlier study also reported protein instability for p.T1030I (31). Finally, p.G937 and p.G1043 are examples of glycine residues that provide structural flexibility at the beginning of a loop structure (Fig. 4c, Supplementary Fig. 10). Changing these residues into a larger and charged arginine (p.G937R) or aspartate (p.G1043D), will lead to deformation of the loop structure and probable loss of surrounding hydrogen bonds in the case of p.G1043D. Altogether, this *in silico* modeling may provide explanations for how these PALB2 VUS affect protein stability/expression levels. Nonetheless, some VUS for which similar destabilizing effects are predicted (p.D871G, p.L931R, p.E1018D and p.W1164C) are fully functional in our HR-based assays, underpinning the importance of functional analysis of VUS.

VUS in the PALB2 CC-domain disrupt the interaction with BRCA1

In addition to the damaging VUS in PALB2's WD40 domain, we also found 4 PALB2 VUS (p.L24S, p.Y28C, p.L35P, p.R37H) exhibiting strong effects on HR and PARPi sensitivity (Figs. 2a and 3a, Supplementary Fig. 6). These variants were all located in PALB2's N-terminal coiled-coil domain, which is required for interaction with BRCA1 (6,9). Indeed, the previously reported p.Y28C and p.L35P variants affected HR by impairing the interaction with BRCA1 (30). However, exactly how p.L24S and p.R37H impact HR is unclear, also because p.R37H has previously been reported not to affect the PALB2-BRCA1 interaction (30). To examine this further, we transiently expressed YFP-tagged PALB2 carrying p.L24S, p.L35P or p.R37H in U2OS cells and performed pull-downs using GFP Trap beads. p.L24S, similar to p.L35P, failed to co-precipitate any endogenous BRCA1, whereas p.R37H partially affected the co-precipitation of BRCA1 (Fig. 5a). Additionally, we examined whether these VUS have

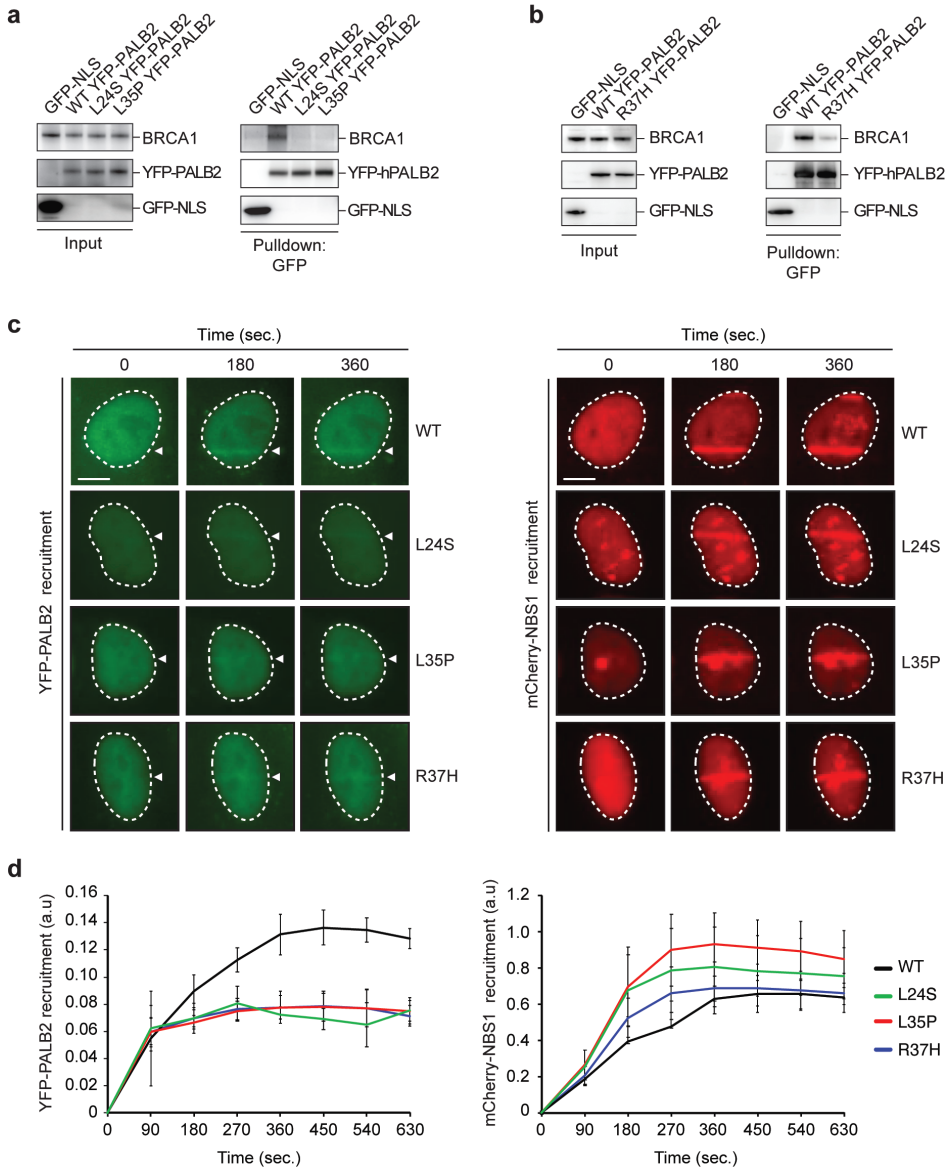

Figure 5. Effect of PALB2 VUS on the BRCA1 interaction and recruitment to DNA damage sites. **a** YPF/GFP pulldowns of the indicated proteins following transient expression in U2OS cells. GFP-NLS and YFP-PALB2-L35P served as negative controls. Western blot analysis was performed using antibodies against GFP and BRCA1. **b** As in **a**, except for p.R37H. **c** Live cell imaging of the recruitment of the indicated YFP-PALB2 proteins to DNA damage tracks generated by laser micro-irradiation in U2OS cells. mCherry-Nbs1, which was co-expressed with the indicated YPF-PALB2 proteins, served as a DNA damage marker. Representative images are shown. White triangles indicate irradiated regions. Scale bars: 5 µm. **d** Quantification of the recruitment of the indicated YPP-PALB2 proteins and mCherry-Nbs1 to DNA damage tracks in cells from. Data represent the mean values (± SEM) from 3 independent experiments. **c**. Source data are provided as a Source Data file.

an impact on the BRCA1-dependent localization of PALB2 to sites of DNA damage. To this end, YFP-tagged PALB2 carrying p.L24S, p.L35P or p.R37H were transiently expressed in U2OS cells and examined for their localization at DNA damage-containing tracks generated by laser micro-irradiation. We found that all three VUS impaired the recruitment of PALB2 to sites of DNA damage (Fig. 5c,d). The effect of these VUS on PALB2's interaction with BRCA1 and localization at sites of DNA damage are highly consistent with the observed HR defect (Figs. 2b and 3a, Supplementary Fig. 6). Taken together, we identified p.L24S and R37H as VUS that impair PALB2's function in HR by abrogating its interaction with BRCA1, and consequently its BRCA1-dependent recruitment to DNA damage sites.

***PALB2* VUS affect G2/M-phase progression after DNA damage**

While PALB2 is essential for HR, two independent genetic screens identified *PALB2* as a critical regulator of the DNA damage-induced G2/M checkpoint response (38,39). Another study demonstrated that *PALB2* plays a role in maintaining a proper G2/M checkpoint response in human cancer cells exposed to ionizing radiation (IR) (40). We therefore addressed if VUS in *PALB2* would affect the DNA damage-induced checkpoint by measuring the mitotic fraction of *Trp53*^{KO} and *Trp53*^{KO}/*Palb2*^{KO} mES cells following exposure to IR. One hour after exposure to 3 or 10 Gy of IR, both *Trp53*^{KO} *and Trp53*^{KO}/*Palb2*^{KO} mES cells showed an almost complete loss of mitotic cells, indicating efficient activation of the G2/M checkpoint in both cell types (Fig. 6a). While at 6 hours after 3 Gy of IR the mitotic fraction of both *Trp53*^{KO} and *Trp53*^{KO}/*Palb2*^{KO} mES cells dramatically increased, we only observed this increase in *Trp53*^{KO}/*Palb2*^{KO} mES after exposure to 10 Gy (Fig. 6a). Thus, *PALB2* is also required for the maintenance of the IR-induced G2/M checkpoint in mES cells.

This prompted us to assess the effect of 19 different *PALB2* variants on G2/M checkpoint maintenance. We expressed these variants, which were selected based on their differential impact on HR (Fig. 2a), in *Trp53*^{KO}/*Palb2*^{KO} mES cells and determined the mitotic fraction 6 hours after exposure to 10 Gy of IR. Importantly, expression of wild-type human *PALB2* rescued the G2/M checkpoint maintenance defect observed in *Trp53*^{KO}/*Palb2*^{KO} mES cells, whereas expressing the empty vector or either of two truncating variants (p.Y551X and p.Y1183X) resulted in a checkpoint defect (Fig. 6b). Two benign variants (p.D134N and p.G998E) and 9 different VUS (p.K18R, p.E42K, p.Y408H, p.P707L, p.D871G, p.L931R, p.1018D, p.Y1046C and p.S1058P) that did not impair HR, also did not impact the maintenance of the IR-induced G2/M checkpoint. In contrast, strong defects in G2/M checkpoint maintenance were observed for 3 VUS (p.L35P, p.L961P and p.G1043D) and the synthetic missense variant p.A1025R that also abrogated HR (Fig. 2b), whereas p.R37H and p.L939W exhibited a moderate effect (Fig. 6b), consistent with their mild impact on HR (Fig.

2b). Accordingly, we found a strong correlation between the impact of *PALB2* variants on HR and G2/M checkpoint maintenance (R^2=*0.8577)* (Fig. 6c). Interestingly, p.L35P and p.A1025R have been shown to abrogate the interaction of PALB2 with BRCA1 (Fig. 5a) (30) and BRCA2 (29), respectively. This indicates that both the interaction with BRCA1 and BRCA2 is crucial for PALB2's function in controlling G2/M-phase progression following DNA damage, which is in accordance with observations in human cancer cells (40).

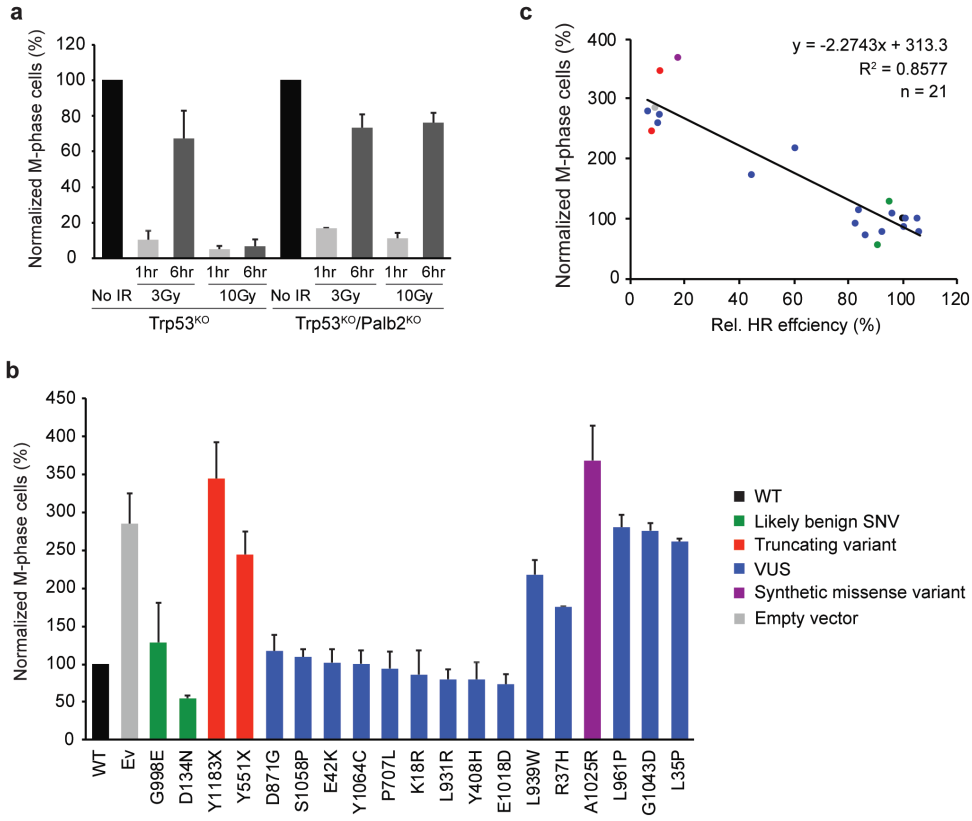

Figure 6. Effect of *PALB2* variants on the DNA damage-induced G2/M checkpoint. a *Trp53*^{KO}/*Palb2*^{KO} mES cells were irradiated with 3 or 10 Gy of IR and collected at the indicated time points after radiation exposure to assess the mitotic index by phospho-histone H3 (Ser10) staining and flowcytometry analysis. Data represent the mean percentage of mitotic cells (± SEM) relative to the unirradiated cells, which was set to 100%, from 2 independent experiments. **b** *Trp53*^{KO}/*Palb2*^{KO} mES cells expressing the indicated *PALB2* variants were irradiated with 10 Gy of IR and collected 6 hours after radiation exposure to assess the mitotic index by phospho-histone H3 (Ser10) staining and flowcytometry analysis. For each variant, the mean percentage of mitotic cells (± SEM) from 2 independent experiments is shown relative to unirradiated cells, except for p.L939W and p.G998E for which data from three independent experiments is presented. **c** Scatter plot showing the correlation between the HR efficiencies and the mitotic index after IR as measured in Fig. 2b and **b**, respectively.

Variants/conditions are categorized by color as in **b**. The trendline indicates the negative correlation between the HR efficiency and mitotic index after IR, revealing a strong positive correlation between the impact of *PALB2* variants on HR and G2/M checkpoint maintenance. Source data are provided as a Source Data file.

Functional analysis of *PALB2* VUS in human cell-based assays

To validate results from our mES cell-based assays, we selected 5 LOF VUS located in the WD40 domain of PALB2 (p.W912G, p.G937R, p.L947S, p.L961P and p.G1043D) and tested their effect on HR in human cell-based assays. To this end, we first employed the CRISPR-LMNA HR assay, which monitors the integration of mRuby, into the Lamin A/C locus (LMNA) by CRISPR/Cas9-mediated HR (Supplementary Fig. 11a,b) (41). Following siRNA-mediated knockdown of *PALB2* in U2OS cells, plasmids encoding the mRuby2-LMNA donor, Cas9 and a *LMNA* gRNA, and siRNA-resistant YFP-PALB2 with or without VUS, were co-transfected into these cells (Supplementary Fig. 11c). Four PALB2 VUS (p.W912G, p.G937R, p.L961P and p.G1043D) showed a dramatic impact on the HR-mediated integration of mRuby (Fig. 7a). One VUS (p.L947S), had a moderate effect, although this is likely explained by the slightly higher transient expression of this variant (Supplementary Fig. 11c). We then assessed whether these VUS would affect PARPi sensitivity. To this end, siRNA-resistant YFP-PALB2 constructs carrying these VUS were expressed in PALB2-depleted HeLa cells (Supplementary Fig. 11d). Four PALB2 VUS (p.W912G, p.G937R, p.L961P and p.G1043D), showed a dramatic increase in PAPRi sensitivity, while 1 VUS (p.L947S) had a more moderate effect, consistent with findings from the CRISPR-LMNA HR assay (Fig. 7b). Altogether, these results corroborate our findings from the DR-GFP and PARPi sensitivity assays in mES cells (Figs. 2a and 3a, Supplementary Fig. 6).

Finally, PALB2 drives HR by promoting the accumulation of RAD51 at DSB sites. To further assess the impact of the 5 selected VUS on PALB2, we examined whether they affected the accumulation of RAD51 at IR-induced DSBs by measuring the formation RAD51 foci. HeLa cells were treated with siRNAs against endogenous *PALB2* and complemented by transient expression of siRNA-resistant YFP-PALB2, with or without VUS. Following exposure to IR, the average number of RAD51 foci was scored in cyclin-A- and YFP-PALB2-expressing S-phase cells (Fig. 7c,d). While 3 VUS (p.W912G, p.L961P and p.G1043D) had a dramatic impact on the percentage of cells showing RAD51 foci, 2 VUS (p.G937R and p.L947S) displayed a more minor effect. However, for these 2 VUS, we found that the intensity of RAD51 foci was dramatically reduced (Fig. 7e). As all 5 variants displayed problems in protein stability in mES cells, we believe that the defects observed in RAD51 foci formation and/or intensity mostly stem from impaired RAD51 recruitment due to reduced PALB2 protein levels. Overall, our findings in human cell-based assays solidify those obtained in the mES cell-based assays,

indicating that our system in mES cells is robust and suited for semi-high throughput functional analysis of VUS in human *PALB2*.

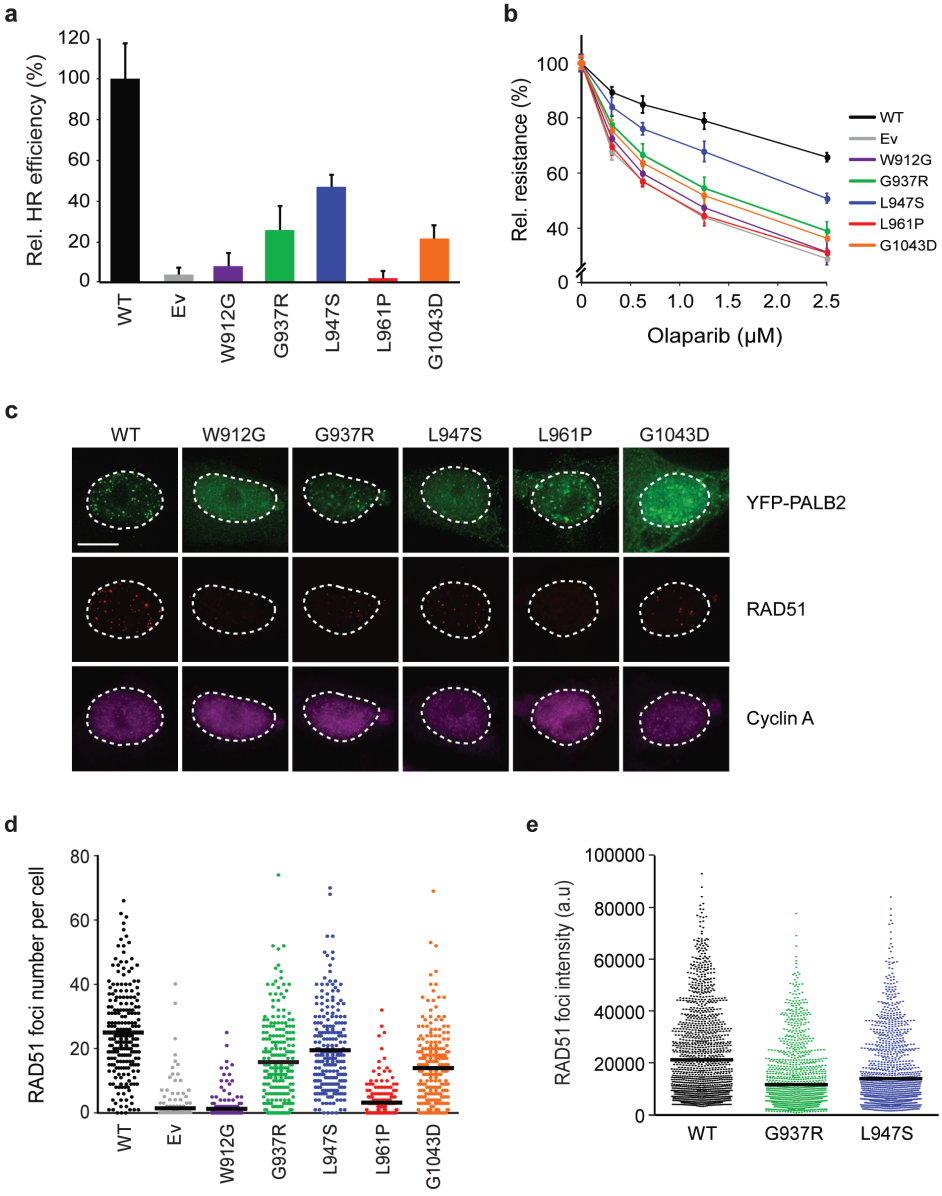

Figure 7. Functional analysis of damaging *PALB2* variants in human cells. a CRISPR-LMNA HDR assay in siRNA-treated U2OS *PALB2* knockdown cells expressing siRNA-resistant human *PALB2* cDNA with the indicated variants (or an empty vector control, Ev). Data represent the mean percentage (± SD) of mRuby2-positive cells among the YFP-positive cells from 3 independent experiments (n >300 YFP-positive cells per condition) relative to wild type (WT), which was set to 100%. **b** PARP inhibitor

(PARPi) sensitivity assay using siRNA-treated HeLa *PALB2* knockdown cells expressing siRNA-resistant human *PALB2* cDNA with the indicated variants (or an empty vector control, Ev). Survival curves were determined after 72 hours of PARPi treatment. Data represent the mean percentage of viability relative to untreated cells (± SD), which was set to 100%, of 3 independent experiments, each performed in triplicate. **c** Representative images of RAD51 foci 4 hours after 2 Gy of ionizing radiation in siRNA-treated HeLa *PALB2* knockdown cells expressing siRNA-resistant human *PALB2* cDNA with the indicated variants (or an empty vector control, Ev). Scale bar: 5 µm. **d** Quantification of the results from **c**. Scatter dot plot shows the number of RAD51 foci in cyclin A-positive cells expressing the indicated variant, with the horizontal lines designating the mean values (± SD) of 3 independent experiments (n>200 cells per condition). **e** Quantification of the results from **c**. Scatter dot plot shows the intensity of RAD51 foci in cyclin A-positive cells expressing the indicated variant, with the horizontal lines designating the mean values (± SD) of 3 independent experiments (n>500 cells per condition). Source data are provided as a Source Data file.

DISCUSION

To address the impact of *PALB2* VUS on protein function, we developed a mES cell-based system that allows a rapid and robust functional classification of genetic variants in human *PALB2*. Out of the 49 PALB2 missense variants tested in this study (Supplementary Data 1), we identified 15 variants (p.L24S, p.Y28C, p.L35P, p.W912G, p.G937R, p.I944N, p.L947S, p.L961P, p.L972Q, p.A1025R, p.T1030I, p.I1037T, p.G1043D, p.L1070P, p.L1172P) as damaging, reducing HR by >60%. For three variants that have been described previously (p.Y28C, p.L35P and p.T1030I), our results are highly consistent with published data, showing that these variants which confer increased risk for breast cancer, strongly impact HR (30,31). Furthermore, we observed a strong positive correlation between the DR-GFP and PARPi or cisplatin sensitivity assays, suggesting that carriers of the identified damaging VUS may benefit from PARPi- or cisplatin-based treatment. Lastly, our data from the human cell-based assays further verify the results from the mES-based cell assays, indicating that our system in mES cells is well-suited for the rapid, semi-high throughput functional analysis of VUS in human PALB2.

In addition to p.Y28C and p.L35P, which have both been reported to impair the interaction with BRCA1 (30), p.R37H also resides in the N-terminal coiled-coil domain and impairs the HR activity by more than 55% in our DR-GFP assay (Fig. 2b). In contrast to an earlier report showing that p.R37H did not affect the interaction with BRCA1 (30), we found that this variant impaired the PALB2-BRCA1 interaction and the BRCA1-dependent recruitment of PALB2 to sites of DNA damage, which is highly consistent with its moderate impact on HR. Our results on the identified p.L24S variant, are in line with a previous study in which the CC6 PALB2 variant, for which the amino acids LKK at position 24-26 are changed to AAA, impairs the interaction with BRCA1 and consequently abrogates HR (42). Thus, our HR and protein-protein association studies for both p.L24S and p.L35P further underline the importance of the BRCA1-PALB2 interaction for efficient HR and likely tumor suppression.

The C-terminal WD40 domain of PALB2 is an important regulatory platform that mediates interactions with several important HR pathway components, such as BRCA2 and RAD51. Crystal structure studies of the WD40 domain showed that it forms a seven-bladed β-propeller-like structure of which correct folding is crucial for PALB2 function (29). As such, it is likely that variants in this region are prone to interfere with the structure and/or biochemical properties of this domain. For example, although it has been reported that p.W1038X exposes a nuclear export signal leading to cytoplasmic localization (43), we see in our assays that the expression levels of this variant are dramatically reduced compared to wild-type PALB2 (Fig. 4a), probably due to instability/misfolding and rapid degradation in the cytoplasm. Indeed, we see similar effects for three other truncating variants (p.Q899X, p.P1009Lfs, p.Y1183X), which includes p.Y1183X that lacks only the last 3 amino acids. Consistent with the WD40 domain being prone to 'destabilizing' variants, we identified 11 damaging VUS in the WD40 domain that exhibited strongly reduced PALB2 protein levels, and consequently strongly reduced HR (~60-95%). Importantly, 5 of these 11 VUS are *bona fide* null variants that abrogate the HR activity to the same extent as the *PALB2* truncating variants. These results indicate that that the WD40 domain is a 'hotspot' for deleterious LOF variants that affect protein stability. Consistently, a recent study on PTEN, showed that 64% of the pathogenic missense variants reduce its expression level (44). This suggests that protein instability due to LOF variants in tumor suppressor genes, including *PALB2,* constitutes a mechanism of pathogenicity.

Several studies have implicated *BRCA1*, *BRCA2* and *PALB2* in DNA-damage-induced checkpoint control (38-40). Accordingly, we found that G2/M checkpoint maintenance after IR is compromised in $Trp53^{KO}/Palb2^{KO}$ mES cells, an effect that could be rescued by expressing wild-type human *PALB2*. Interestingly, *PALB2* variants that show LOF in HR, were unable to maintain an efficient G2/M checkpoint response. Both p.L35P and p.A1025R, which are unable to interact with BRCA1 and BRCA2, respectively, were among these variants, suggesting that these interactions are key to PALB2's checkpoint function. Moreover, we infer that the observed defects in G2/M checkpoint maintenance could stem from defective HR. In line with such a scenario, an inverse correlation has been observed between HR activity and POLQ-mediated DSB repair (45). This indicates that POLQ-mediated DSB repair may act as a compensatory pathway for PALB2-dependent HR that potentially affects G2/M checkpoint maintenance in response to DNA breaks.

Although our functional assays may aid in the classification of rare *PALB2* VUS, a major challenge will be to translate effects on PALB2 protein function into estimates for cancer risk. Whereas the truncating *PALB2* variants have been associated with an odds ratio of 7.46 (5), the p.L939W variant has been associated with an odds ratio of 1.05 (46). This would suggest that a decrease of 40% in HR in our DR-GFP assay, as shown for the p.L939W variant (Fig. 2b), would barely increase the risk for breast cancer. It will therefore be interesting to see

whether the extent to which variants affect HR is proportional to increased cancer risk and at which level of HR deficiency, cancer risk significantly increases. Finally, it will be important to examine whether *PALB2* VUS, either in coding or non-coding sequences, affect *PALB2* splicing. For all missense variants presented in this study *in silico* splice site prediction analysis was performed using five different algorithms (Splice Site Finder-like, MaxEntScan, GeneSplicer, NNSplice, Human Splicing Finder) in Alamut (http://www.interactive-biosoftware.com/). For all VUS an effect on RNA splicing was unlikely, with the exception of c.53A>G (p.K18R) for which NNSplice predicted the introduction of a new weak acceptor recognition site in exon 2. Complementation of our *Trp53*^{KO}/*Palb2*^{KO} cells with a bacterial artificial chromosome (BAC) containing the full length human *PALB2* gene, as has been previously described for *BRCA1* and *BRCA2* (14,47,48), would also enable us to address the functional effect of splice variants in *PALB2*. Ultimately, the results from functional assays for VUS can be incorporated into multifactorial risk models to allow for better clinical classification in the future. Indeed, multiple pieces of evidence, in addition to functional assay results, will be required to enable clinical classification of VUS.

MATERIALS AND METHODS

Cell lines and culture conditions

129/Ola E14 IB10 mES cells (49) were cultured on gelatin-coated dishes in 50% BRL/50% complete medium (13) with 0.1 mM beta-mercaptoethanol (Merck) and 10^3 Units/ml ESGRO LIF (Millipore). STR genotyped U2OS and HeLa human cells (ATCC) were maintained, respectively, in McCoy's 5A (Wisent) and DMEM (ThermoFischer) supplemented with 10% Fetal Bovine Serum (FBS) and 1% penicillin and streptomycin.

Generation of *Trp53*^{KO}/*Palb2*^{KO} mES cells with DR-GFP and RMCE

Trp53^{KO}/*Palb2*^{KO} mES cells carrying the DR-GFP reporter and RMCE system were generated as follows. 75 µg of the plasmids carrying *Pim1*:DR-GFP (p59X DRGFP) (50) or the *Rosa26:* RMCE acceptor cassette (pTT5-Puro) (TaconicArtemis GmbH) were linearized with *Xho*I and *Pvu*I respectively. *Pim1*:DR-GFP was transfected into mES cells (49) using Lipofectamine 2000 (Invitrogen). Integration of DR-GFP at *Pim1* was verified using PCR and Southern blot analysis. Similarly, the RMCE acceptor cassette was integrated at *Rosa26* in cells carrying DR-GFP. Integration of the RMCE acceptor cassette at *Rosa26* was verified using PCR and Southern blot analysis. *Trp53*^{KO} cells were generated by transfection of 1 µg of pSpCas9(BB)-2A-GFP (*pX458*) (51), which encodes a gRNA that targets exon 1 (5'-CGAGCTCCCTCTGAGCCAGG-3'), into mES cells carrying DR-GFP and the RMCE acceptor

cassette. GFP-positive cells were FACS-sorted and seeded. Individual clones were examined by TIDE and western blot analysis for loss of p53 expression. Similarly, the *Palb2*^{KO} was generated in *Trp53*^{KO} mES cells carrying DR-GFP and RMCE acceptor cassette using a gRNA that targets exon 4 (5'-GGGGACAACAAAGACGCCGT-3'), and verified by TIDE and western blot analysis for loss of Palb2 expression.

Cloning and site-directed mutagenesis of human *PALB2* cDNA

pBudCE4.1 (ThermoFisher, V53220), which contains an EF1α promotor, was modified by cloning two different oligonucleotides with *Pac*I restriction sites into the *Nhe*I (5'-CTAGGACTTAATTAAGTCGATCGCCGG-3') and *Bgl*II restriction sites (5'-GATCTCTTAATTAAGACTG-3'), respectively. Human Flag-tagged *PALB2* cDNA was obtained from pcDNA3-Flag-PALB2 and subcloned into pBudCE4.1-*Pac*I using the *Acc*65I and *Xho*I restriction sites. An Ef1α-*PALB2*-containing fragment from pBudCE4.1-*Pac*I-PALB2 was then cloned into the RMCE vector pRNA 251-MCS RMCE) (TaconicArtemis GmbH) using the *Pac*I restriction sites in both vectors. *PALB2* variants were introduced by site-directed mutagenesis using the Quick-Change Lightning protocol (Agilent Technologies). Constructs were verified by Sanger sequencing and used for mES cell-based assays. For human cell-based assays, siRNA-resistant pEYFP-PALB2 construct was generated by site-directed mutagenesis using the Q5 Site-Directed Mutagenesis Kit (New England Biolabs) as per the manufacturer's protocol with the following primers: forward primer - 5'-GATCTTATTGTTCTACCAGGAAAATC-3' and reverse primer - 5'-TTCCTCTAAGTCCTCCATTTCTG-3'. PALB2 variants were introduced in the siRNA-resistant pEYFP-C1-PALB2 plasmid by site-directed mutagenesis using the same kit. All primers used for site-directed mutagenesis are listed in Supplementary Data 1.

Karyotyping

mES cells (50% confluency) were incubated with 0.05 µg/ml colcemid (Gibco) for 2.5 hours. After trypsinization, 2.5 ml of 0.4% Na-citrate, 0.4% KCL (1:1) was added in a dropwise manner. Cells were centrifuged at 120 g after which the supernatant was aspirated and 2.5 ml fixative consisting of methanol and acidic acid (4:1) was added while slowly vortexing. This step was repeated twice. Using ultrathin pipet tips, a small number of cells was dropped onto a cleaned microscopy slide (VWR, 631-1551) and left to air-dry. DAPI was used for visualizing the chromosomes, which were counted using a Zeiss microscope Imager M2 (63x) and ZEN 2012 microscopy software.

Western blot analysis

Expression of endogenous mouse PALB2 and human PALB2 in mES was monitored by

protein extraction and western blot. Briefly, samples were generated by taking up ~1.5x10^6 cells in 75 µl Laemmli buffer and boiling them at 95°C for 5 minutes. Samples were incubated with 1.5 µl benzonase (Merck Millipore 70746-3, 25 U/µl) for 10 minutes at room temperature and then loaded for gel electrophoresis and immunoblotting. Primary antibodies used were a rabbit polyclonal antibody against the N-terminus of human PALB2 (1:1000, kindly provided by Cell Signaling Technology prior to commercialization), a homemade rabbit antibody against the N-terminus of mouse PALB2 (42) (NB3 anti-mPalb2, 1:2000, kind gift form Bing Xia) and a mouse monoclonal antibody against alpha tubulin (1:10000, Sigma, T6199 clone DM1A). Peroxidase-AffiniPure Goat Anti-Rabbit secondary antibody (Jackson laboratories) and SuperSignal West Femto Maximum Sensitivity Substrate (ThermoFisher) were used for development of blots on the Amersham Imager 600 (GE Healthcare Life Sciences).
Western blotting was performed by separating U2OS and HeLa protein extracts on 12% SDS-PAGE gels at 100V and transferred to nitrocellulose membrane during 1.5 hour at 100V. Membranes were blocked for 1 hour in 5% milk in Tris-buffered saline (TBS)-Tween. Primary antibodies applied were mouse monoclonal anti-GFP (1:1000, Roche, #11814460001**),** anti-alpha tubulin (1:200000, Abcam, #ab7291) and a home-made rabbit polyclonal antibody against human PALB2 (1:5000). Horseradish peroxidase-conjugated anti-mouse IgG (1:10000, Jackson ImmunoResearch) were used as secondary antibodies.

RT-qPCR analysis

RNA was isolated from mES cells on 6-well plates using Trizol (ThermoFisher, 15596026) as per the manufacturer's protocol. For each condition, 3 µg RNA was treated with RQ1 RNAse-free DNAse (Promega, M6101) and cDNA was synthesized from 0.2 µg DNAse-treated RNA using hexamer primers (ThermoFisher, N8080127) and AMV Reverse Transcriptase (ThermoFisher, 12328019) as per the manufacturer's protocols. RT-qPCRs were carried out using GoTaq qPCR Master mix (Promega, A6002), a CFX384 Real-Time System (Bio-Rad) and the following qPCR primers directed at the human *PALB2* cDNA or the mouse control gene *Pim1*; PALB2-Fw - 5'-GATTACAAGGATGACGACGATAAGATGGAC-3', PALB2-Rv - 5'-CCTTTTCAAGAATGCTAATTTCTCCTTTAACTTTTCC-3'. Pim1-exon4-Fw - 5'-GCGGCGAAATCAAACTCATCGAC-3' and Mouse Pim1-exon5-Rv - 5'-GTAGCGATGGTAGCGAATCCACTCTGG-3'.

HR Reporter Assays

2x10^6 *Trp53*^{KO}*/Palb2*^{KO} mES cells carrying the DR-GFP reporter and RMCE system were subjected to RMCE by co-transfecting 1 µg FlpO expression vector (pCAGGs-FlpO-IRES-puro) (19) with 1 µg RMCE exchange vector. Neomycin-resistant cells from ~500 resistant clones were pooled and expanded for DR-GFP reporter assays. 1 µg of a plasmid for co-

expression of I-SceI and mCherry (pCMV-Red-Isce, kind gift from Jos Jonkers) was transfected in $1x10^6$ cells using Lipofectamine 2000 (ThermoFisher) (13). A co-transfection of 1 µg pCAGGs (53) with 0.05 µg of an mCherry expression vector was included as control. Two days after transfection, mCherry/GFP double-positive cells were scored using a Novocyte Flow Cytometer (ACEA Biosciences, Inc.).

For the CRISPR-LMNA HR assay (43), U2OS cells were seeded in 6-well plates at $2x10^5$ cells per well. Knockdown of *PALB2* was performed 6 hours later with 50 nM siRNA against PALB2 (5'-CUUAGAAGAGGACCUUAUU-3'; Dharmacon) using Lipofectamine RNAiMAX (Invitrogen). Twenty-four hours post-transfection, $1.5x10^6$ cells were pelleted for each condition and resuspended in 100 µl complete nucleofector solution (SE Cell Line 4D-Nucleofector™ X Kit, Lonza) to which 1µg of pCR2.1-mRuby2LMNAdonor, 1 µg pX330-LMNAgRNA, 1 µg peYFP-C1 or the indicated siRNA-resistant YFP-PALB2 construct, and 150 pmol siRNA was added. Once transferred to a 100 µl Lonza certified cuvette, cells were transfected using the 4D-Nucleofector X-unit, program CM-104 and transferred to a 10 cm dish. After 48 hours, cells were trypsinized and plated onto glass coverslips. Cells were fixed with 4% paraformaldehyde and analyzed for mRuby2 and YFP expression on a Leica CTR 6000 inverted microscope using a 63x/1.40 oil immersion objective 72 hours post-nucleofection.

PARPi and cisplatin sensitivity assays

For proliferation-based PARPi and cisplatin sensitivity assays, mES cells were seeded in triplicate at 10.000 cells per well of a 96-well plate. The next day, cells were treated with PARP inhibitor Olaparib (Selleckchem, S1060) or cisplatin (Accord Healthcare, 15683354) for two days, after which the medium was refreshed and cells were cultured for one more day. Viable cells were subsequently counted using the Novocyte Flow Cytometer (ACEA Biosciences, Inc.).

For clonogenic PARPi survival assays, mES cells were seeded on p60 plates at the following densities: 250 cells without PARPi, 400 cells for functional variants with 1 or 5 nM PARPi, and 3000 cells for damaging variants with 1 or 5 nM PARPi. Cells were treated for 7-9 days allowing the visible formation of surviving colonies which were counted following methylene blue staining (2.5 gr/L in 5% ethanol). HeLa cells were seeded at 240000 cells per well of a 6-well plate before being transfected 6 hours later with 50 nM control or *PALB2* siRNA using Lipofectamine RNAiMAX (Invitrogen). The next day, cells were complemented with 0.8 µg of EYFP-PALB2 plasmid DNA using Lipofectamine 2000 (Invitrogen) for 24 hours and then seeded in triplicates into a Corning 3603 black-sided clear bottom 96-well microplate at a density of 3000 cells per well. After 3 days of treatment with Olaparib (Selleckchem, S1060), nuclei were stained with Hoechst 33342 (Invitrogen) at 10 µg/ml in media for 45 minutes at

37°C. Images of entire wells were acquired at 4x with a Cytation 5 Cell Imaging Multi-Mode Reader followed by quantification of Hoechst-stained nuclei with the Gen5 Data Analysis Software v3.03 (BioTek Instruments).

Cell cycle analysis and G2/M checkpoint assays

For cell cycle profile analysis cells were fixed in 70% ethanol. After 15 minutes incubation on ice, cells were pelleted and resuspended in 500 µl PBS containing 50 µg/ml propidium iodide (PI) (ThermoFisher, P1304MP), 0.1 mg/ml RNase A and 0.05% Triton X-100, followed by 40 minutes incubation at 37°C. Cells were then washed with PBS and analyzed using the Novocyte Flow Cytometer (ACEA Biosciences, Inc.).

For G2/M checkpoint assays, $1x10^6$ mES cells were seeded on p60 dishes one day before exposure to 3 or 10 Gy of IR. One or 6 hours later, cells were fixed as described for cell cycle profile analysis and incubated overnight at -20°C. Fixed cells were then permeabilized for 15 minutes on ice using 0.25% Triton X-100 in PBS, after which mitotic cells were stained in 100 µl PBS with 1 µl anti-phospho-H3 Ser10 (1µg/µl, Sigma-Aldrich, 06-570) for 3 hours at room temperature. Alexa-488 goat α-rabbit (1:100 in 100µl PBS; ThermoFisher, 11034) was used as a secondary antibody. Cells were analyzed using the Novocyte Flow Cytometer (ACEA Biosciences, Inc.).

Pulldown assays

20 µg YFP-PALB2 plasmid DNA (previously described (54)) was transfected into ~$10x10^6$ U2OS cells on a 15 cm dish using Lipofectamine 2000. The next day cells were trypsinized, washed with cold PBS, and transferred to LoBind Eppendorf tubes. Cells were then lysed in 1 ml EBC buffer (50 mM Tris pH 7.3, 150 mM NaCl, 0.5% NP-40, 2.5 mM $MgCl_2$), containing 1 tablet protease inhibitor (Roche) per 10 ml buffer. 500 Units benzonase was then added to each condition and cells were incubated for 60 minutes at 4 °C on a rotating wheel. The lysate was subsequently centrifuged for 10 minutes at 18400 g at 4°C. The supernatant was then added to 25 µl of pre-washed GFP-trap beads (ChromoTek) in LoBind Eppendorf tubes and incubated for 1.5 hours at 4 °C on a rotating wheel. The beads were washed 5-6 times with EBC buffer with spinning steps of 1 minute at 3380 g at 4°C. Beads were eventually resuspended in 25 µl Laemmli buffer after which about half of each sample was analyzed by western blot analysis using a homemade rabbit antibody against human BRCA1 (55) (1:1000, kind gift form Dan Durocher).

Laser micro-irradiation and PALB2 recruitment

U2OS cells were grown on 18-mm coverslips and sensitized with 10 μM 5′ -bromo-2-deoxyuridine (BrdU) for 24 h before micro-irradiation. Cells were co-transfected with 1 μg pYFP-PALB2, with or without a variant, and 0.5 μg mCherry-NBS1 expression vector using lipofectamine 2000 (Invitrogen). For micro-irradiation, cells were placed in a live-cell imaging chamber set to 37 °C in CO2-independent Leibovitz's L15 medium supplemented with 10% FCS and penicillin–streptomycin (Invitrogen). Live cell imaging and micro-irradiation experiments were carried out with a Zeiss Axio Observer microscope driven by ZEN software using a 63x/1.4 oil immersion objective coupled to a 355 nm pulsed DPSS UV-laser (Rapp OptoElectronic). To monitor the recruitment of YFP-PALB2 to laser-induced DNA damage sites, cells were imaged before and after laser irradiation at 90 seconds time intervals over a period of 10.5 minutes. The fluorescence intensity of YFP-PALB2 and mCherry-NBS1 at DNA damage sites relative to that in an unirradiated region of the nucleus was quantified and plotted over time. Kinetic curves were obtained by averaging the relative fluorescence intensity of cells displaying positive recruitment (n>30 cells per condition).

RAD51 foci analysis

HeLa cells were seeded on glass coverslips in 6-well plates at 225.000 cells per well. Knockdown of *PALB2* was performed 18 hours later with 50 nM PALB2 siRNA using Lipofectamine RNAiMAX (Invitrogen). After 5 hours, cells were subjected to a double thymidine block. Briefly, cells were treated with 2 mM thymidine for 18 hours and released into fresh medium for 9 hours. During the release time, 0.8 μg YFP-PALB2 plasmid DNA (with or without variant) was transfected into the cells using Lipofectamine 2000. Cells were then treated with 2 mM thymidine for 17 hours and protected from light from this point on. After 2 hours of release from the second block, cells were irradiated with 2 Gy and processed for immunofluorescence 4 hours post-irradiation. Unless otherwise stated, all immunofluorescence dilutions were prepared in PBS and incubations performed at room temperature with intervening washes in PBS. Cell fixation was carried out by incubation with 4% paraformaldehyde for 10 minutes followed by 100% ice-cold methanol for 5 minutes at -20 °C. This was succeeded by permeabilization in 0.2% Triton X-100 for 5 minutes and a quenching step using 0.1% sodium borohydride for 5 minutes. After blocking for 1 hour in a solution containing 10% goat serum and 1% BSA, cells were incubated for 1 hour with primary antibodies anti-RAD51 (1 :7000, B-bridge International, #70-001) and anti-cyclin A (1 :400, BD Biosciences, # 611268) diluted in 1% BSA. Secondary antibodies Alexa Fluor 568 goat anti-rabbit (Invitrogen, #A-11011) and Alexa Fluor 647 goat anti-mouse (Invitrogen, #A-21235) were diluted 1 :1000 in 1% BSA and applied for 1 hour. Nuclei were stained for 10 minutes with 1 μg/mL DAPI prior to mounting onto slides with 90% glycerol containing 1 mg/ml paraphenylenediamine anti-fade reagent. Z-

stack images were acquired at 63X magnification on a Leica CTR 6000 microscope, then deconvolved and analyzed for RAD51 foci. The number and intensity of RAD51 foci in cyclin A-positive cells expressing the indicated YFP-PALB2 constructs were scored using automatic spot counting in Volocity software v6.0.1 (Perkin-Elmer Improvision).

DATA AVAILABILITY

All data generated or analysed during this study are included in this published article (and its supplementary information files).

AUTHOR CONTRIBUTIONS

R.B. cloned *PALB2* cDNA in the RMCE exchange construct, generated *PALB2* variants using site-directed mutagenesis, generated *Trp53*^{KO}/*Palb2*^{KO} mES cells harboring the DR-GFP reporter and RMCE acceptor cassette, and performed DR-GFP, PARPi, Cisplatin, G2/M checkpoint, and pull-down assays, as well as Southern and western blot analysis, and PCR and DNA sequencing analysis in mES cells. Amélie Rodrigue generated YFP-PALB2 variants using site-directed mutagenesis and performed CRISPR-LMNA HR, PARPi sensitivity and RAD51 foci assays, as well as western blot analysis in human cells. C.S. assisted with the PARPi assays in mES cells. W.W. performed G2/M checkpoint assays. B.V. performed *in silico* modeling of *PALB2* variants. M.S. generated PALB2 p.A1025R using site-directed mutagenesis and performed DR-GFP and PARPi proliferation assays for this variant. M.R. studied YFP-PALB2 recruitment to laser-induced DNA damage. N.C. performed cell cycle profile analysis in mES cells. M.V. helped with gathering *PALB2* variants from databases and literature and assisted in the *in silico* analysis. F.C. provided p.L24S, p.I944N and p.L1070P variants. J.S. and J.-Y.M. supervised experiments performed in human cells. M.V., P.D. and H.v.A. conceived the project. H.v.A. supervised the project. R.B and H.v.A. wrote the paper.

COMPETING INTERESTS

The authors declare no competing interests.

ACKNOWLEDGEMENTS

The authors would like to thank Jos Jonkers and Peter Bouwman for providing the pTT5-Puro (RMCE acceptor cassette), pRNA-251-MCS (RMCE exchange vector) and pCMV-Red-I-Sce constructs, as well as Dan Durocher and Bing Xia for sharing BRCA1 and PALB2 antibodies,

respectively. We are grateful to Maria Jasin and Francis Stewart for sharing the DR-GFP reporter and FlpO constructs, respectively. We thank Patrick van Vliet and Richard Lemmers for help with the Southern blot analysis, and Cell Signaling and Dan Durocher for providing antibodies directed against PALB2 and BRCA1, respectively. Finally, we would like to thank Jamie Allen and the BRIDGES consortium for providing *PALB2* variants. This work was financially supported by the Government of Canada through Genome Canada and the Canadian Institutes of Health Research, the Ministère de l'Économie, de la Science et de l'Innovation du Québec through Genome Québec and the Quebec Breast Cancer Foundation (J.S. and J.-Y.M.), as well as by grants from the Ministère de l'Économie, de la Science et de l'Innovation du Québec through the PSR-SIIRI-949 program (J.S. and J.-Y.M), the CIHR (Foundation grant to J.-Y.M), European Union (BRIDGES grant to P.D., M.V. and H.v.A.) and the Dutch Cancer Society (P.D. and H.v.A.).

REFERENCES

1. Antoniou A, Pharoah PD, Narod S, Risch HA, Eyfjord JE, Hopper JL*, et al.* Average risks of breast and ovarian cancer associated with BRCA1 or BRCA2 mutations detected in case Series unselected for family history: a combined analysis of 22 studies. American journal of human genetics **2003**;72(5):1117-30 doi 10.1086/375033.
2. Rahman N, Seal S, Thompson D, Kelly P, Renwick A, Elliott A*, et al.* PALB2, which encodes a BRCA2-interacting protein, is a breast cancer susceptibility gene. Nature genetics **2007**;39(2):165-7 doi 10.1038/ng1959.
3. Reid S, Schindler D, Hanenberg H, Barker K, Hanks S, Kalb R*, et al.* Biallelic mutations in PALB2 cause Fanconi anemia subtype FA-N and predispose to childhood cancer. Nature genetics **2007**;39(2):162-4 doi 10.1038/ng1947.
4. Antoniou AC, Casadei S, Heikkinen T, Barrowdale D, Pylkas K, Roberts J*, et al.* Breast-cancer risk in families with mutations in PALB2. The New England journal of medicine **2014**;371(6):497-506 doi 10.1056/NEJMoa1400382.
5. Couch FJ, Shimelis H, Hu C, Hart SN, Polley EC, Na J*, et al.* Associations Between Cancer Predisposition Testing Panel Genes and Breast Cancer. JAMA Oncol **2017**;3(9):1190-6 doi 10.1001/jamaoncol.2017.0424.
6. Zhang F, Fan Q, Ren K, Andreassen PR. PALB2 functionally connects the breast cancer susceptibility proteins BRCA1 and BRCA2. Molecular cancer research : MCR **2009**;7(7):1110-8 doi 10.1158/1541-7786.MCR-09-0123.
7. Zhang F, Ma J, Wu J, Ye L, Cai H, Xia B*, et al.* PALB2 links BRCA1 and BRCA2 in the DNA-damage response. Curr Biol **2009**;19(6):524-9 doi 10.1016/j.cub.2009.02.018.
8. Xia B, Sheng Q, Nakanishi K, Ohashi A, Wu J, Christ N*, et al.* Control of BRCA2 cellular and clinical functions by a nuclear partner, PALB2. Molecular cell **2006**;22(6):719-29 doi 10.1016/j.molcel.2006.05.022.
9. Sy SM, Huen MS, Chen J. PALB2 is an integral component of the BRCA complex required for homologous recombination repair. Proceedings of the National Academy of Sciences of the United States of America **2009**;106(17):7155-60 doi 10.1073/pnas.0811159106.
10. Polak P, Kim J, Braunstein LZ, Karlic R, Haradhavala NJ, Tiao G*, et al.* A mutational signature reveals alterations underlying deficient homologous recombination repair in breast cancer. Nature genetics **2017**;49(10):1476-86 doi 10.1038/ng.3934.
11. Farmer H, McCabe N, Lord CJ, Tutt AN, Johnson DA, Richardson TB*, et al.* Targeting the DNA repair defect in BRCA mutant cells as a therapeutic strategy. Nature **2005**;434(7035):917-21 doi 10.1038/nature03445.
12. Buisson R, Dion-Cote AM, Coulombe Y, Launay H, Cai H, Stasiak AZ*, et al.* Cooperation of breast cancer proteins PALB2 and piccolo BRCA2 in stimulating homologous recombination. Nature structural & molecular biology **2010**;17(10):1247-54 doi 10.1038/nsmb.1915.

13. Bouwman P, van der Gulden H, van der Heijden I, Drost R, Klijn CN, Prasetyanti P*, et al.* A high-throughput functional complementation assay for classification of BRCA1 missense variants. Cancer discovery **2013**;3(10):1142-55 doi 10.1158/2159-8290.CD-13-0094.
14. Mesman RLS, Calleja F, Hendriks G, Morolli B, Misovic B, Devilee P*, et al.* The functional impact of variants of uncertain significance in BRCA2. Genetics in medicine : official journal of the American College of Medical Genetics **2018** doi 10.1038/s41436-018-0052-2.
15. Shimelis H, Mesman RLS, Von Nicolai C, Ehlen A, Guidugli L, Martin C*, et al.* BRCA2 Hypomorphic Missense Variants Confer Moderate Risks of Breast Cancer. Cancer research **2017**;77(11):2789-99 doi 10.1158/0008-5472.CAN-16-2568.
16. Findlay GM, Daza RM, Martin B, Zhang MD, Leith AP, Gasperini M*, et al.* Accurate classification of BRCA1 variants with saturation genome editing. Nature **2018**;562(7726):217-22 doi 10.1038/s41586-018-0461-z.
17. Starita LM, Islam MM, Banerjee T, Adamovich AI, Gullingsrud J, Fields S*, et al.* A Multiplex Homology-Directed DNA Repair Assay Reveals the Impact of More Than 1,000 BRCA1 Missense Substitution Variants on Protein Function. American journal of human genetics **2018**;103(4):498-508 doi 10.1016/j.ajhg.2018.07.016.
18. Kass EM, Helgadottir HR, Chen CC, Barbera M, Wang R, Westermark UK*, et al.* Double-strand break repair by homologous recombination in primary mouse somatic cells requires BRCA1 but not the ATM kinase. Proceedings of the National Academy of Sciences of the United States of America **2013**;110(14):5564-9 doi 10.1073/pnas.1216824110.
19. Kranz A, Fu J, Duerschke K, Weidlich S, Naumann R, Stewart AF*, et al.* An improved Flp deleter mouse in C57Bl/6 based on Flpo recombinase. Genesis **2010**;48(8):512-20 doi 10.1002/dvg.20641.
20. Rantakari P, Nikkila J, Jokela H, Ola R, Pylkas K, Lagerbohm H*, et al.* Inactivation of Palb2 gene leads to mesoderm differentiation defect and early embryonic lethality in mice. Hum Mol Genet **2010**;19(15):3021-9 doi 10.1093/hmg/ddq207.
21. Bouwman P, Drost R, Klijn C, Pieterse M, van der Gulden H, Song JY*, et al.* Loss of p53 partially rescues embryonic development of Palb2 knockout mice but does not foster haploinsufficiency of Palb2 in tumour suppression. J Pathol **2011**;224(1):10-21 doi 10.1002/path.2861.
22. Blomen VA, Majek P, Jae LT, Bigenzahn JW, Nieuwenhuis J, Staring J*, et al.* Gene essentiality and synthetic lethality in haploid human cells. Science **2015**;350(6264):1092-6 doi 10.1126/science.aac7557.
23. Greenblatt MS, Chappuis PO, Bond JP, Hamel N, Foulkes WD. TP53 mutations in breast cancer associated with BRCA1 or BRCA2 germ-line mutations: distinctive spectrum and structural distribution. Cancer research **2001**;61(10):4092-7.
24. Rhei E, Bogomolniy F, Federici MG, Maresco DL, Offit K, Robson ME*, et al.* Molecular genetic characterization of BRCA1- and BRCA2-linked hereditary ovarian cancers. Cancer research **1998**;58(15):3193-6.

25. Li A, Geyer FC, Blecua P, Lee JY, Selenica P, Brown DN*, et al.* Homologous recombination DNA repair defects in PALB2-associated breast cancers. NPJ Breast Cancer **2019**;5:23 doi 10.1038/s41523-019-0115-9.
26. Xia B, Dorsman JC, Ameziane N, de Vries Y, Rooimans MA, Sheng Q*, et al.* Fanconi anemia is associated with a defect in the BRCA2 partner PALB2. Nature genetics **2007**;39(2):159-61 doi 10.1038/ng1942.
27. Susswein LR, Marshall ML, Nusbaum R, Vogel Postula KJ, Weissman SM, Yackowski L*, et al.* Pathogenic and likely pathogenic variant prevalence among the first 10,000 patients referred for next-generation cancer panel testing. Genetics in medicine : official journal of the American College of Medical Genetics **2016**;18(8):823-32 doi 10.1038/gim.2015.166.
28. Kraus C, Hoyer J, Vasileiou G, Wunderle M, Lux MP, Fasching PA*, et al.* Gene panel sequencing in familial breast/ovarian cancer patients identifies multiple novel mutations also in genes others than BRCA1/2. International journal of cancer **2017**;140(1):95-102 doi 10.1002/ijc.30428.
29. Oliver AW, Swift S, Lord CJ, Ashworth A, Pearl LH. Structural basis for recruitment of BRCA2 by PALB2. EMBO reports **2009**;10(9):990-6 doi 10.1038/embor.2009.126.
30. Foo TK, Tischkowitz M, Simhadri S, Boshari T, Zayed N, Burke KA*, et al.* Compromised BRCA1-PALB2 interaction is associated with breast cancer risk. Oncogene **2017**;36(29):4161-70 doi 10.1038/onc.2017.46.
31. Park JY, Singh TR, Nassar N, Zhang F, Freund M, Hanenberg H*, et al.* Breast cancer-associated missense mutants of the PALB2 WD40 domain, which directly binds RAD51C, RAD51 and BRCA2, disrupt DNA repair. Oncogene **2014**;33(40):4803-12 doi 10.1038/onc.2013.421.
32. Michl J, Zimmer J, Tarsounas M. Interplay between Fanconi anemia and homologous recombination pathways in genome integrity. The EMBO journal **2016**;35(9):909-23 doi 10.15252/embj.201693860.
33. Adzhubei IA, Schmidt S, Peshkin L, Ramensky VE, Gerasimova A, Bork P*, et al.* A method and server for predicting damaging missense mutations. Nat Methods **2010**;7(4):248-9 doi 10.1038/nmeth0410-248.
34. Sim NL, Kumar P, Hu J, Henikoff S, Schneider G, Ng PC. SIFT web server: predicting effects of amino acid substitutions on proteins. Nucleic Acids Res **2012**;40(Web Server issue):W452-7 doi 10.1093/nar/gks539.
35. Tavtigian SV, Deffenbaugh AM, Yin L, Judkins T, Scholl T, Samollow PB*, et al.* Comprehensive statistical study of 452 BRCA1 missense substitutions with classification of eight recurrent substitutions as neutral. J Med Genet **2006**;43(4):295-305 doi 10.1136/jmg.2005.033878.
36. Rentzsch P, Witten D, Cooper GM, Shendure J, Kircher M. CADD: predicting the deleteriousness of variants throughout the human genome. Nucleic Acids Res **2019**;47(D1):D886-D94 doi 10.1093/nar/gky1016.

37. Ioannidis NM, Rothstein JH, Pejaver V, Middha S, McDonnell SK, Baheti S*, et al.* REVEL: An Ensemble Method for Predicting the Pathogenicity of Rare Missense Variants. American journal of human genetics **2016**;99(4):877-85 doi 10.1016/j.ajhg.2016.08.016.
38. Cotta-Ramusino C, McDonald ER, 3rd, Hurov K, Sowa ME, Harper JW, Elledge SJ. A DNA damage response screen identifies RHINO, a 9-1-1 and TopBP1 interacting protein required for ATR signaling. Science **2011**;332(6035):1313-7 doi 10.1126/science.1203430.
39. Menzel T, Nahse-Kumpf V, Kousholt AN, Klein DK, Lund-Andersen C, Lees M*, et al.* A genetic screen identifies BRCA2 and PALB2 as key regulators of G2 checkpoint maintenance. EMBO reports **2011**;12(7):705-12 doi 10.1038/embor.2011.99.
40. Simhadri S, Vincelli G, Huo Y, Misenko S, Foo TK, Ahlskog J*, et al.* PALB2 connects BRCA1 and BRCA2 in the G2/M checkpoint response. Oncogene **2019**;38(10):1585-96 doi 10.1038/s41388-018-0535-2.
41. Ducy M, Sesma-Sanz L, Guitton-Sert L, Lashgari A, Gao Y, Brahiti N*, et al.* The Tumor Suppressor PALB2: Inside Out. Trends Biochem Sci **2019** doi 10.1016/j.tibs.2018.10.008.
42. Simhadri S, Peterson S, Patel DS, Huo Y, Cai H, Bowman-Colin C*, et al.* Male fertility defect associated with disrupted BRCA1-PALB2 interaction in mice. The Journal of biological chemistry **2014**;289(35):24617-29 doi 10.1074/jbc.M114.566141.
43. Pauty J, Couturier AM, Rodrigue A, Caron MC, Coulombe Y, Dellaire G*, et al.* Cancer-causing mutations in the tumor suppressor PALB2 reveal a novel cancer mechanism using a hidden nuclear export signal in the WD40 repeat motif. Nucleic Acids Res **2017**;45(5):2644-57 doi 10.1093/nar/gkx011.
44. Matreyek KA, Starita LM, Stephany JJ, Martin B, Chiasson MA, Gray VE*, et al.* Multiplex assessment of protein variant abundance by massively parallel sequencing. Nature genetics **2018**;50(6):874-82 doi 10.1038/s41588-018-0122-z.
45. Ceccaldi R, Liu JC, Amunugama R, Hajdu I, Primack B, Petalcorin MI*, et al.* Homologous-recombination-deficient tumours are dependent on Poltheta-mediated repair. Nature **2015**;518(7538):258-62 doi 10.1038/nature14184.
46. Southey MC, Goldgar DE, Winqvist R, Pylkas K, Couch F, Tischkowitz M*, et al.* PALB2, CHEK2 and ATM rare variants and cancer risk: data from COGS. J Med Genet **2016**;53(12):800-11 doi 10.1136/jmedgenet-2016-103839.
47. Kuznetsov SG, Liu P, Sharan SK. Mouse embryonic stem cell-based functional assay to evaluate mutations in BRCA2. Nat Med **2008**;14(8):875-81 doi 10.1038/nm.1719.
48. Chang S, Biswas K, Martin BK, Stauffer S, Sharan SK. Expression of human BRCA1 variants in mouse ES cells allows functional analysis of BRCA1 mutations. J Clin Invest **2009**;119(10):3160-71 doi 10.1172/JCI39836.
49. Robanus-Maandag E, Dekker M, van der Valk M, Carrozza ML, Jeanny JC, Dannenberg JH*, et al.* p107 is a suppressor of retinoblastoma development in pRb-deficient mice. Genes & development **1998**;12(11):1599-609.
50. Moynahan ME, Pierce AJ, Jasin M. BRCA2 is required for homology-directed repair of chromosomal breaks. Molecular cell **2001**;7(2):263-72.

51. Ran FA, Hsu PD, Wright J, Agarwala V, Scott DA, Zhang F. Genome engineering using the CRISPR-Cas9 system. Nature protocols **2013**;8(11):2281-308 doi 10.1038/nprot.2013.143.
52. Cruz C, Castroviejo-Bermejo M, Gutierrez-Enriquez S, Llop-Guevara A, Ibrahim YH, Gris-Oliver A*, et al.* RAD51 foci as a functional biomarker of homologous recombination repair and PARP inhibitor resistance in germline BRCA-mutated breast cancer. Ann Oncol **2018**;29(5):1203-10 doi 10.1093/annonc/mdy099.
53. Niwa H, Yamamura K, Miyazaki J. Efficient selection for high-expression transfectants with a novel eukaryotic vector. Gene **1991**;108(2):193-9.
54. Bleuyard JY, Buisson R, Masson JY, Esashi F. ChAM, a novel motif that mediates PALB2 intrinsic chromatin binding and facilitates DNA repair. EMBO reports **2012**;13(2):135-41 doi 10.1038/embor.2011.243.
55. Noordermeer SM, Adam S, Setiaputra D, Barazas M, Pettitt SJ, Ling AK*, et al.* The shieldin complex mediates 53BP1-dependent DNA repair. Nature **2018**;560(7716):117-21 doi 10.1038/s41586-018-0340-7.

SUPPLEMENTARY INFORMATION

Functional analysis of genetic variants in the high-risk breast cancer susceptibility gene *PALB2*

Rick A.C.M. Boonen, Amélie Rodrigue, Chantal Stoepker, Wouter W. Wiegant, Bas Vroling, Milan Sharma, Magdalena B. Rother, Nandi Celosse, Maaike P.G. Vreeswijk, Fergus Couch, Jacques Simard, Peter Devilee, Jean-Yves Masson and Haico van Attikum.

The supplementary information contains:

- Supplementary Data 1
- Supplementary Figure 1-11

Supplementary Data 1. Complete list of human *PALB2* variants analyzed in this study.

Protein change	Mutation type	Prior classification	Align GVGD	CADD (phred)	PolyPhen	SIFT	REVEL	HR (%)	PARPi (%)	Cispl. (%)	Norm. M-phase (%)
p.P4S	Missense	VUS	C0	16,53	0,09	0,35	0,04	97,61	72,70	X	X
p.P5S	Missense	VUS	C0	16,21	0,02	0,49	0,03	62,31	95,74	X	X
p.K18R	Missense	VUS	C0	24,30	1,00	0,03	0,18	100,19	94,47	84,05	86,76
p.L24S*	Missense	VUS	C65	23,80	1,00	0,01	0,17	20,67	55,40	X	X
p.Y28C*	Missense	VUS	C65	26,70	1,00	0,01	0,22	32,92	21,70	X	X
p.T31I	Missense	VUS	C65	26,50	1,00	0,01	0,21	97,16	102,22	X	X
p.L35P*	Missense	VUS	C65	31,00	1,00	0,10	0,35	10,40	9,68	26,03	260,91
p.R37H	Missense	VUS	C25	24,20	0,97	0,01	0,16	44,90	67,82	83,16	175,61
p.E42K	Missense	VUS	C15	34,00	1,00	0,02	0,14	105,41	94,84	89,72	101,81
p.Q60Rfs	Frameshift	Pathogenic	X	X	X	X	X	8,55	11,06	X	X
p.D134N	Missense	Likely benign	C0	10,56	0,02	0,47	0,04	90,64	93,44	97,73	54,70
p.S172fs	Frameshift	Pathogenic	X	X	X	X	X	8,55	13,87	X	X
p.P210L	Missense	Likely benign	C0	9134,00	0,02	0,66	0,10	85,37	102,70	X	X
p.E230X	Nonsense	Pathogenic	X	X	X	X	X	7,42	17,50	X	X
p.L337S	Missense	Likely benign	C0	11,35	0,29	0,23	0,04	86,67	115,71	X	X
p.Y408H	Missense	VUS	C65	29,40	1,00	N/A	-	92,32	108,51	93,33	79,77
p.Y409X	Nonsense	Pathogenic	X	X	X	X	X	7,82	17,43	X	X
p.S417Y	Missense	VUS	C15	26,10	1,00	0,00	0,33	72,20	83,96	X	X
p.D498Y	Missense	Likely benign	C0	21,00	0,90	0,07	0,09	94,49	74,18	X	X
p.K515R	Missense	VUS	C0	15,96	0,20	0,15	0,01	75,45	120,54	X	X
p.L531Cfs	Frameshift	Pathogenic	X	X	X	X	X	7,75	23,96	X	X
p.Y551X	Nonsense	Pathogenic	X	X	X	X	X	8,12	10,68	20,08	244,69
p.Q559R	Missense	Likely benign	C0	0,08	0,00	0,75	0,02	95,02	117,58	X	X
p.L622P	Missense	VUS	C65	28,90	1,00	0,01	0,34	77,45	64,92	X	X
p.E669Gfs	Frameshift	Pathogenic	X	X	X	X	X	7,03	19,46	X	X
p.E672Q	Missense	Likely benign	C0	10,78	0,23	0,28	0,03	79,52	103,53	X	X
p.T706I	Missense	VUS	C15	24,40	1,00	0,01	0,25	87,35	78,20	X	X
p.P707L	Missense	VUS	C65	27,70	1,00	0,00	0,33	82,83	87,96	100,97	93,92
p.V858=	Synonymous	Likely benign	X	X	X	X	X	84,43	74,36	X	X
p.P864S	Missense	Likely benign	C0	19,49	0,58	0,38	0,06	85,80	86,54	X	X
p.S865P	Missense	VUS	C0	28,20	1,00	0,03	0,19	100,10	78,30	X	X
p.D871G	Missense	VUS	C35	27,60	1,00	0,02	0,52	84,07	115,45	87,40	116,75
p.C882Wfs	Frameshift	Pathogenic	X	X	X	X	X	6,10	29,04	X	X
p.W912G*	Missense	VUS	C0	25,60	1,00	0,00	0,56	6,66	7,73	X	X
p.D927A	Missense	VUS	C0	32,00	0,96	0,02	0,25	75,71	86,26	X	X
p.L931R	Missense	VUS	C65	27,30	1,00	0,00	0,57	106,25	94,55	112,08	79,77
p.G937R*	Missense	VUS	C65	28,40	1,00	0,00	0,48	17,35	26,39	X	X
p.L939W	Missense	VUS	C55	29,40	1,00	0,00	0,36	60,28	91,12	102,20	218,25

Supplementary Data 1. Continued

Protein change	Mutation type	Prior classification	Align GVGD	CADD (phred)	PolyPhen	SIFT	REVEL	HR (%)	PARPi (%)	Cispl. (%)	Norm. M-phase (%)
p.E940G	Missense	VUS	C65	29,60	1,00	0,00	0,43	63,40	81,17	X	X
p.I944N*	Missense	VUS	C15	26,70	1,00	0,00	0,45	7,27	14,78	X	X
p.L947S*	Missense	VUS	C65	24,90	1,00	0,00	0,38	30,27	24,31	X	X
p.L961P*	Missense	VUS	C25	25,50	1,00	0,02	0,27	6,53	8,41	27,29	280,28
p.I966T	Missense	VUS	C0	26,40	1,00	0,22	0,21	74,49	78,91	X	X
p.L972Q*	Missense	VUS	C35	28,20	1,00	0,00	0,23	14,02	12,77	X	X
p.Q988X	Nonsense	Pathogenic	X	X	X	X	X	6,70	15,23	X	X
p.G998E	Missense	Likely benign	C65	27,70	1,00	0,01	0,29	95,16	97,37	80,44	129,12
p.P1009Lfs	Frameshift	Pathogenic	X	X	X	X	X	6,16	25,09	X	X
p.E1018D	Missense	VUS	C0	23,40	1,00	0,05	0,12	86,41	84,41	111,51	73,37
p.A1025R	Missense	VUS	C65	23,10	1,00	0,05	0,13	17,62	24,27	X	368,90
p.T1030I*	Missense	VUS	C65	31,00	1,00	0,00	0,43	14,68	14,80	X	X
p.I1037T*	Missense	VUS	C25	26,10	1,00	0,00	0,41	38,86	52,23	X	X
p.W1038X	Nonsense	Pathogenic	X	X	X	X	X	6,98	12,35	X	X
p.L1040S	Missense	VUS	C0	31,00	1,00	0,03	0,31	76,97	99,69	X	X
p.G1043D*	Missense	VUS	C65	29,80	1,00	0,00	0,30	10,59	10,42	37,28	275,71
p.I1051S	Missense	VUS	C35	27,30	1,00	0,00	0,22	91,24	108,56	X	X
p.S1058P	Missense	VUS	C0	28,10	0,99	0,01	0,19	95,88	85,13	119,03	108,97
p.Y1064C	Missense	VUS	C65	31,00	1,00	0,00	0,44	101,04	87,27	128,59	100,42
p.L1070P*	Missense	VUS	C65	26,40	1,00	0,00	0,47	23,09	56,67	X	X
p.P1111A	Missense	VUS	C25	28,10	1,00	0,02	0,40	102,61	87,51	X	X
p.L1119P	Missense	VUS	C65	-	1,00	0,00	0,47	94,33	103,83	X	X
p.V1123M	Missense	VUS	C0	26,70	1,00	0,00	0,23	75,85	102,57	X	X
p.L1143H	Missense	VUS	C0	26,70	1,00	0,14	0,22	69,83	98,43	X	X
p.W1159L	Missense	VUS	C0	28,20	1,00	0,01	0,37	90,82	108,27	X	X
p.S1160P	Missense	VUS	C0	26,90	1,00	0,01	0,26	92,22	103,21	X	X
p.W1164C	Missense	VUS	C65	33,00	1,00	0,00	0,43	80,95	96,22	X	X
p.L1172P*	Missense	VUS	C65	28,90	1,00	0,00	0,48	13,46	16,60	X	X
p.G1174R	Missense	VUS	C65	31,00	1,00	0,00	0,43	90,57	102,88	X	X
p.I1180T	Missense	VUS	C25	24,20	1,00	0,01	0,34	81,82	98,64	X	X
p.Y1183C	Missense	VUS	C55	27,90	1,00	0,00	0,41	70,86	109,07	X	X
p.Y1183X	Nonsense	Pathogenic	X	X		X	X	11,12	9,67	19,53	344,61

All variants are indicated at the protein level (i.e., protein change). Nucleotide annotations for each variant are available in the published manuscript, where nucleotide numbering reflects Human Genome Variation Society (HGVS) nomenclature and cDNA number +1 corresponds to the A of the ATG translation initiation codon in the reference sequence (*PALB2* NM_024675.3). The initiation codon is codon 1. In silico predictions, results from DR-GFP, PARPi sensitivity, cisplatin sensitivity and G2/M checkpoint assays in mES cells are included. Strongly damaging variants from the functional assays (HR >60% reduced) are indicated in the 'protein change' column (red *).

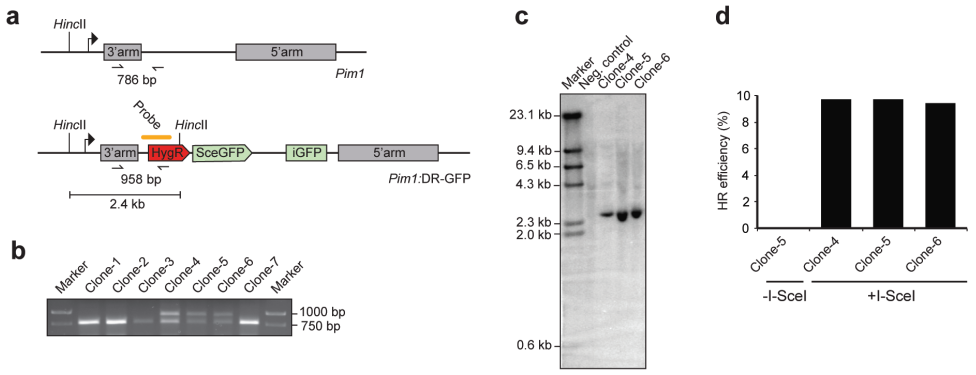

Supplementary Figure 1. Stable integration of the DR-GFP reporter at the *Pim1* locus in mES cells. **a** Schematic showing the *Pim1* locus (upper) and *Pim1* locus with an integrated DR-GFP reporter (*Pim1:*DR-GFP; lower) in mES cells. Integration is directed by the 3' and 5' homology arms. Correct integration of the reporter results in expression of a hygromycin resistance marker under control of the endogenous *Pim1* promoter (not shown). Correct integration was examined by PCR and Southern blot analysis using the indicated primers, as well as probe and restriction enzymes, respectively. **b** PCR analysis of genomic DNA from hygromycin-resistant mES cell clones obtained after targeting the *Pim1* locus with a DR-GFP cassette using primers indicated in A. Clone 4-6 show correct integration of DR-GFP at a *Pim1* allele (as evidence by the appearance of a 958 bp band). **c** Southern blot analysis of *Hinc*II-digested genomic DNA from mES cell clones 4-6 from B using the probe shown in A. Single copy genomic integration at a *Pim1* allele is observed in all three clones (as evidence by the appearance of a 2.4 kb band). **d** DR-GFP assay DR-GFP assay in clone 4-6 from **b** and **c**. Cells were co-transfected with I-SceI and mCherry expression vectors, or mCherry expression vector only, and GFP expression was monitored by FACS. Data represent the absolute percentage of GFP-positive cells among the mCherry-positive-cells. Source data are provided as a Source Data file.

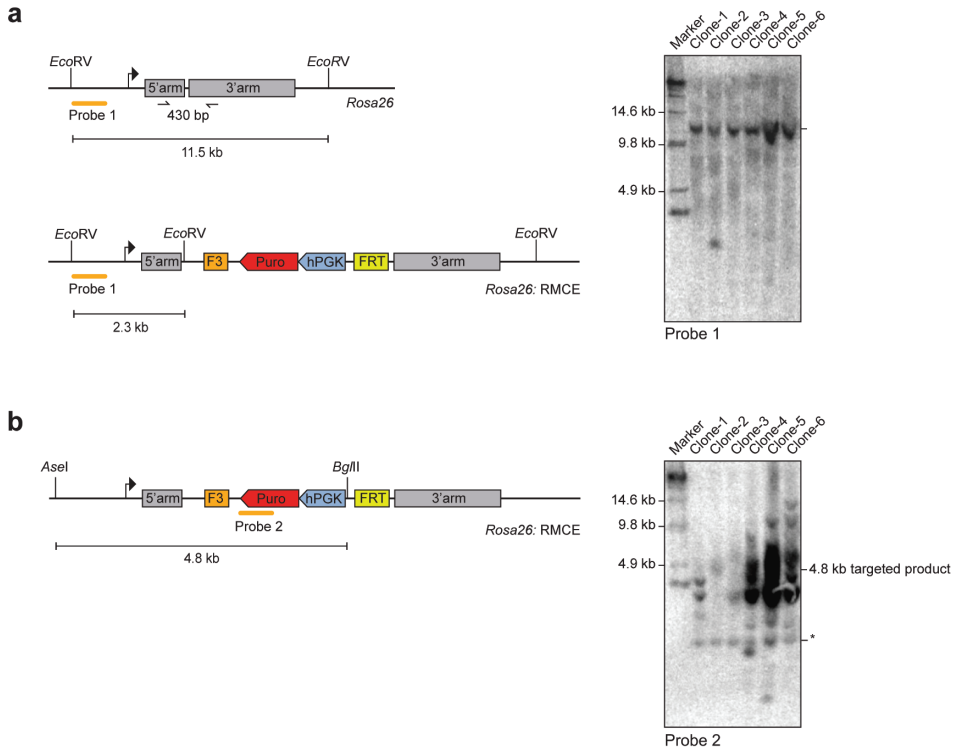

Supplementary Figure 2. Stable integration of the RMCE acceptor cassette at the *Rosa26* locus in mES cells carrying DR-GFP. **a** Schematic showing the *Rosa26* locus (upper left) and *Rosa26* locus with an integrated RMCE acceptor cassette (*Rosa26:*RMCE; lower left) in mES cells. Integration is directed by the 3' and 5' homology arms. Correct integration of the RMCE acceptor cassette results in expression of a puromycin resistance marker under control of the PGK1 promoter. Correct integration was examined by Southern blot analysis of *Eco*RV-digested genomic DNA from mES cell clones 1-6 using the indicated probe (right). Single copy genomic integration at a *Rosa26* allele is observed in clone 2 (as evidence by the appearance of a 2.3 kb band). **b** Schematic as in **a**, except that a different probe and different restriction sites for Southern blot analysis are shown (left). Correct integration was examined by Southern blot analysis of *Ase*I- and *Bgl*II-digested genomic DNA from mES cell clones 1-6 using the indicated probe (right). Single copy genomic integration at a *Rosa26* allele is observed in clone 2 (as evidence by the appearance of a 4.8 kb band).

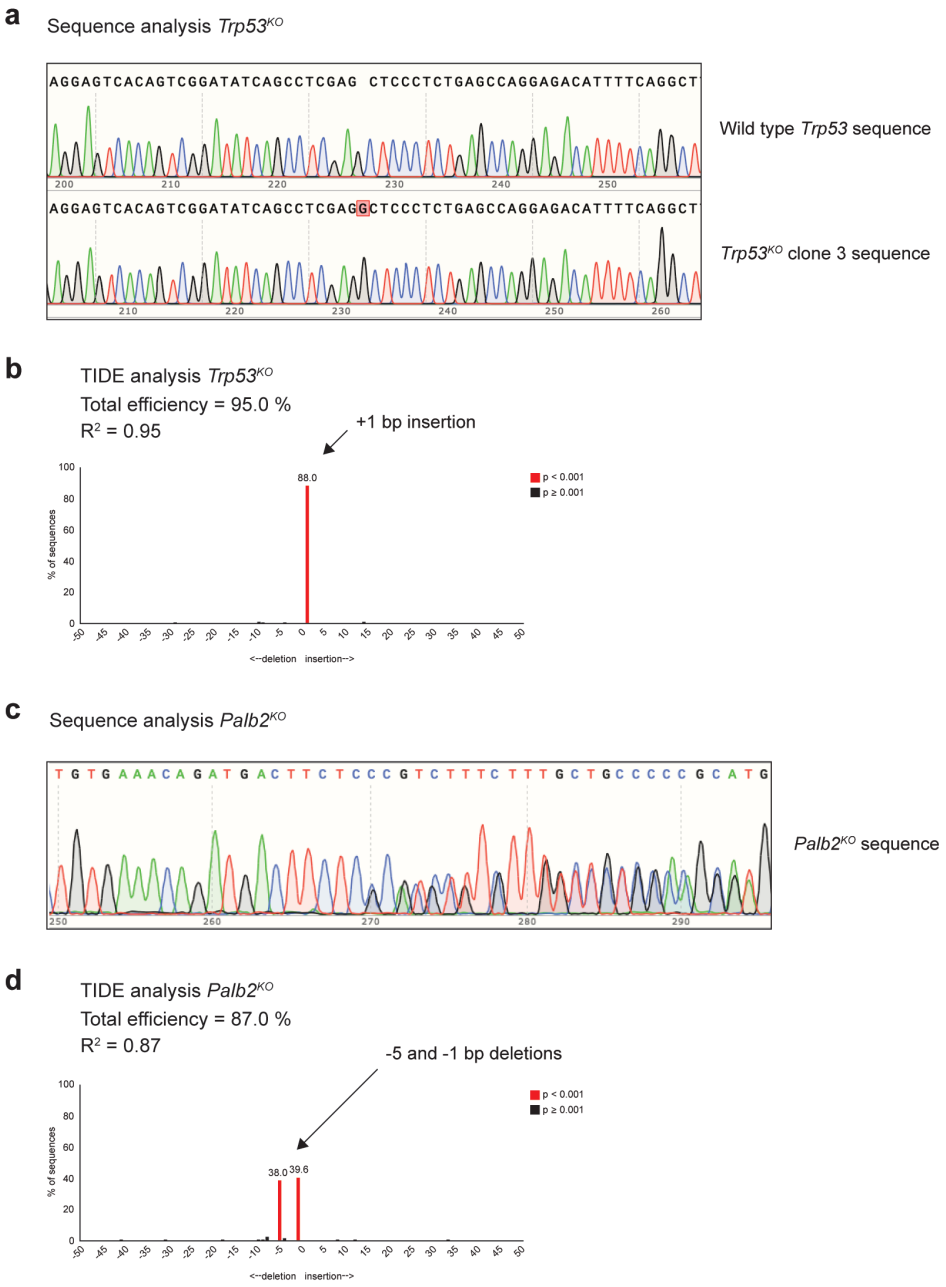

Supplementary Figure 3. Validation of *Trp53*^{KO}/*Palb2*^{KO} mES cells. **A**, Sequence alignment of a fragment of exon 1 of the *Trp53* gene showing a +1 bp (guanine) insertion in *Trp53*^{KO} clone 3. **b** TIDE analysis confirming the +1 bp insertion in exon 1 of the *Trp53* gene in *Trp53*^{KO} clone 3. **c** Sequence alignment of a fragment of exon 4 of the *Palb2* gene showing -5 bp and -1 bp deletions in the *Palb2*^{KO} clone. **d** TIDE analysis confirming -1 and -5 bp deletions in exon 4 of the *Palb2* gene in the *Palb2*^{KO} clone.

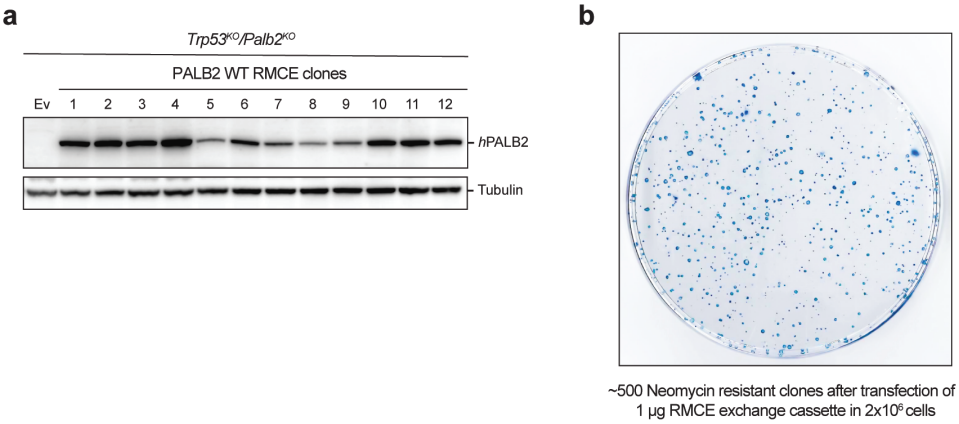

Supplementary Figure 4. RMCE efficiency in mES cells. **a** Western blot analysis of the expression of wild-type human *PALB2* in 12 individual *Trp53*^{KO}/*Palb2*^{KO} mES cell clones using an antibody directed against the N-terminus of PALB2. An empty vector (Ev) served as negative control. Tubulin was used as a loading control. **b** Representative image of a culture dish with methylene-stained neomycin resistant clones after transfection of *Trp53*^{KO}/*Palb2*^{KO} mES cells using RMCE exchange cassette. Source data are provided as a Source Data file.

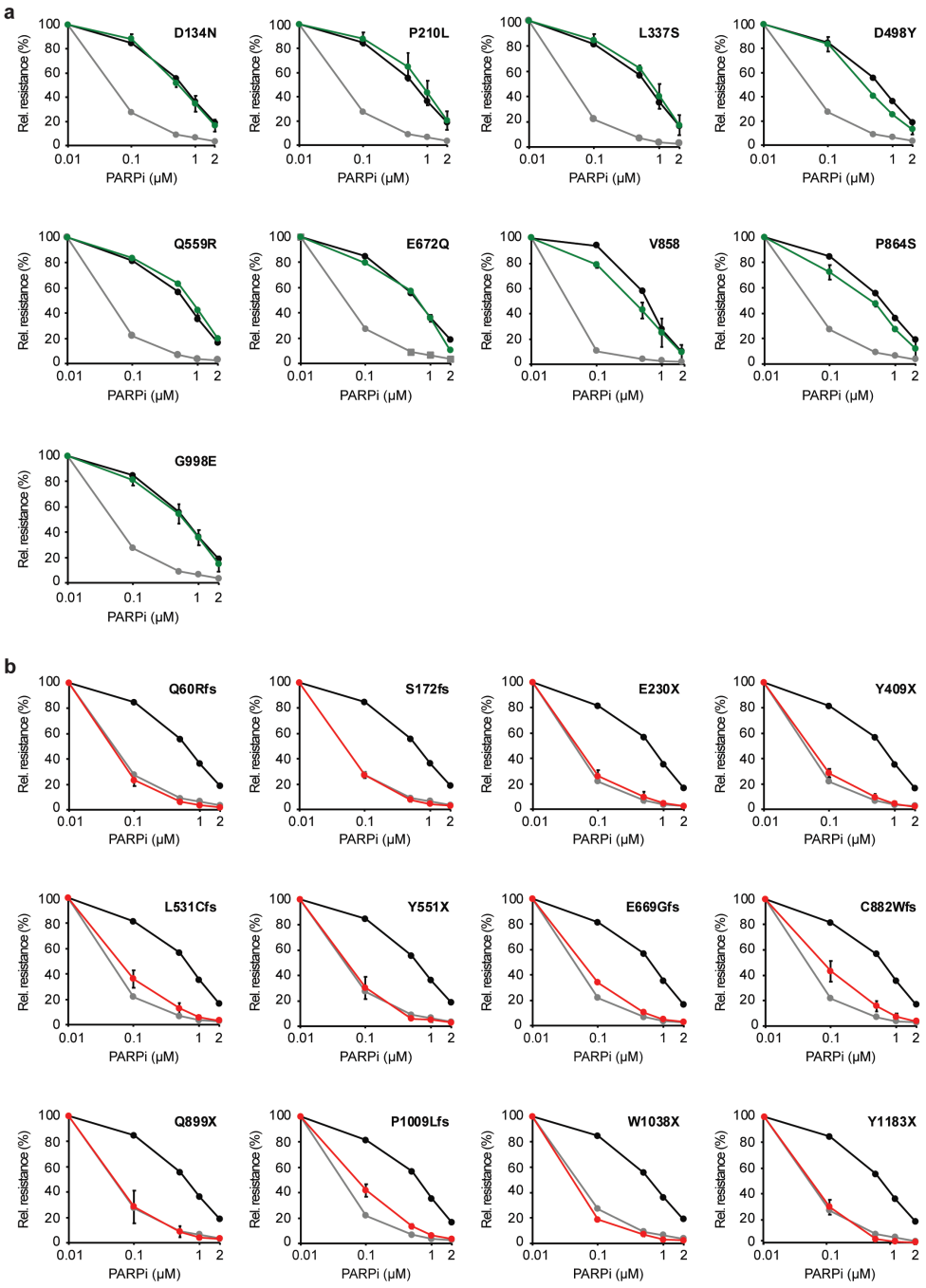
a
D134N
P210L
L337S
D498Y
Q559R
E672Q
V858
P864S
G998E
b
Q60Rfs
S172fs
E230X
Y409X
L531Cfs
Y551X
E669Gfs
C882Wfs
Q899X
P1009Lfs
W1038X
Y1183X
Rel. resistance (%)
PARPi (μM)
0.01
0.1
1
2
0
20
40
60
80
100

Supplementary Figure 5. Functional analysis of benign and truncating variants in human *PALB2* by PARPi sensitivity assays. **a** PARP inhibitor (PARPi) sensitivity assay using *Trp53*^{KO}/*Palb2*^{KO} mES cells expressing human *PALB2* variants (or an empty vector control, Ev). Cells were exposed to the indicated concentrations of PARPi for two days. Cell viability was measured 1 day later using FACS. Data represent the mean percentage of viability/resistance relative to untreated cells (± SEM) from 2 independent experiments, except for p.P210L for which data from three independent experiments is presented. Variants/conditions are categorized by color as either wild type (WT, black), likely benign SNV (green), or empty vector (Ev, grey). Data from the 0.5 μM PARPi concentration are shown in Fig. 3a. **b** as in **a**, except for truncating variants (red). Source data are provided as a Source Data file.

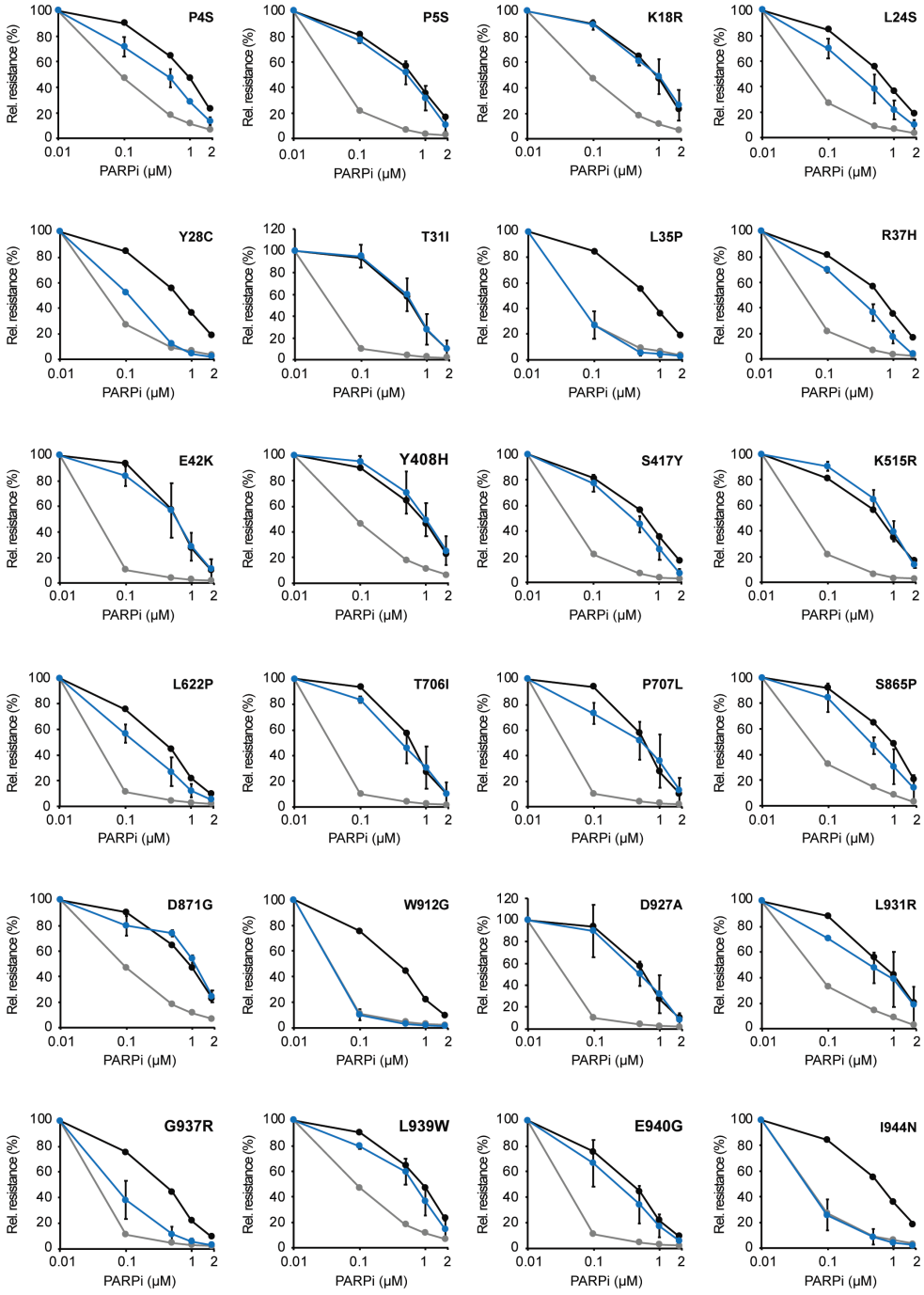
P4S
P5S
K18R
L24S
Y28C
T31I
L35P
R37H
E42K
Y408H
S417Y
K515R
L622P
T706I
P707L
S865P
D871G
W912G
D927A
L931R
G937R
L939W
E940G
I944N
Rel. resistance (%)
PARPi (μM)
0.01
0.1
1
2

Supplementary Figure 6. Functional analysis of selected VUS in human *PALB2* by PARPi sensitivity assays. PARP inhibitor (PARPi) sensitivity assay using *Trp53*^{KO}/*Palb2*^{KO} mES cells expressing human *PALB2* variants (or an empty vector control, Ev). Cells were exposed to the indicated concentrations of PARPi for two days. Cell viability was measured 1 day later using FACS. Data represent the mean percentage of viability/resistance relative to untreated cells (± SEM) from 2 independent experiments, except for p.P4S and p.L939W, for which data from three independent experiments is presented, and p.L24S for which data from four independent experiments is presented. Variants/conditions are categorized by color as either wild type (WT, black), VUS (blue), or empty vector (Ev, grey). Data from the 0.5 μM PARPi concentration are shown in Fig. 3a. Source data are provided as a Source Data file.

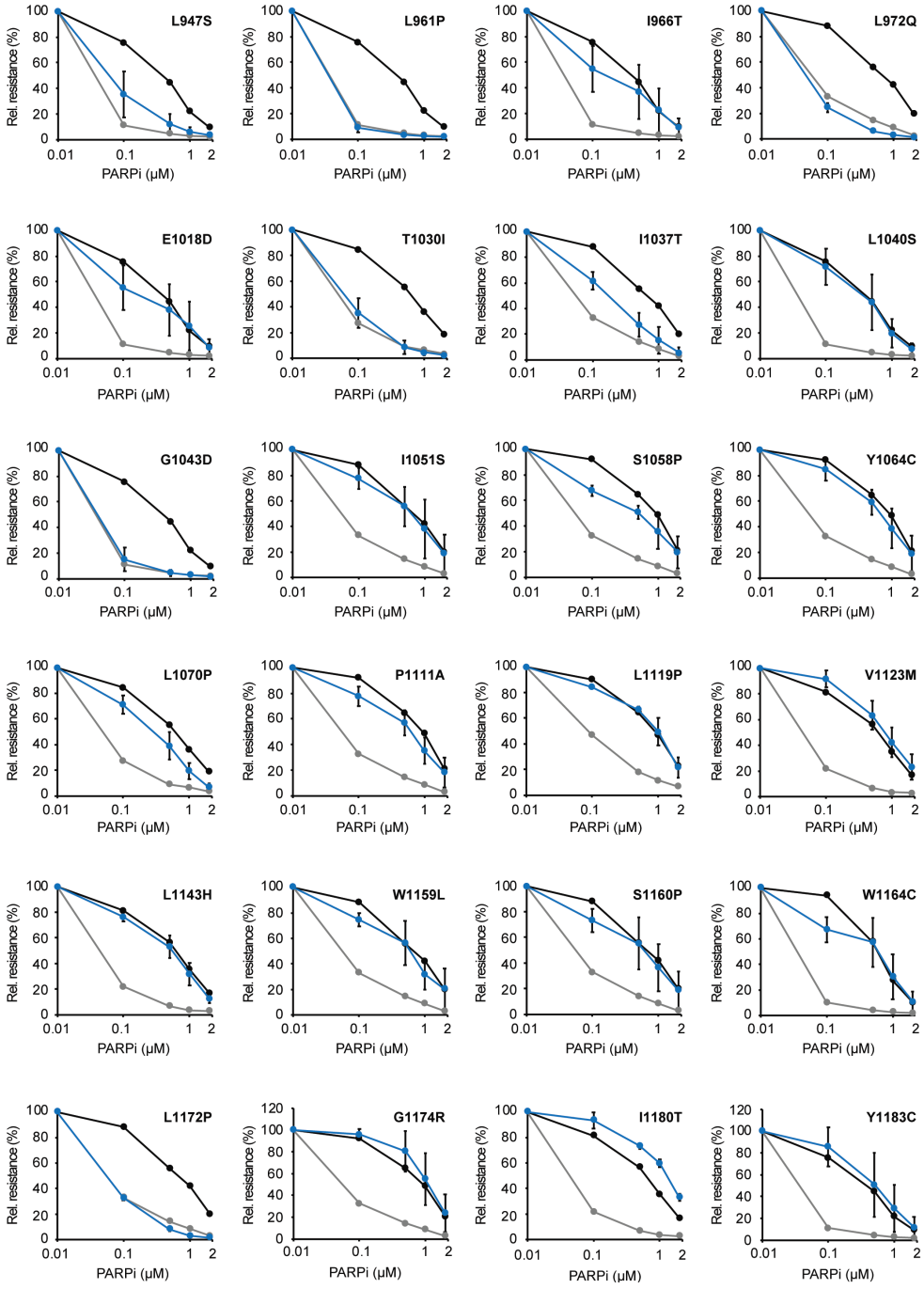
L947S
L961P
I966T
L972Q
E1018D
T1030I
I1037T
L1040S
G1043D
I1051S
S1058P
Y1064C
L1070P
P1111A
L1119P
V1123M
L1143H
W1159L
S1160P
W1164C
L1172P
G1174R
I1180T
Y1183C
Rel. resistance (%)
PARPi (μM)

Supplementary Figure 7. Functional analysis of selected VUS in human *PALB2* by PARPi sensitivity assays. PARP inhibitor (PARPi) sensitivity assay using *Trp53*^{KO}/*Palb2*^{KO} mES cells expressing human *PALB2* variants (or an empty vector control, Ev). Cells were exposed to the indicated concentrations of PARPi for two days. Cell viability was measured 1 day later using FACS. Data represent the mean percentage of viability/resistance relative to untreated cells (± SEM) from 2 independent experiments, except for p.V1123M for which data from three independent experiments is presented, and p.L1070P for which data from four independent experiments is presented. Variants/conditions are categorized by color as either wild type (WT, black), VUS (blue), or empty vector (Ev, grey). Data from the 0.5 μM PARPi concentration are shown in Fig. 3a. Source data are provided as a Source Data file.

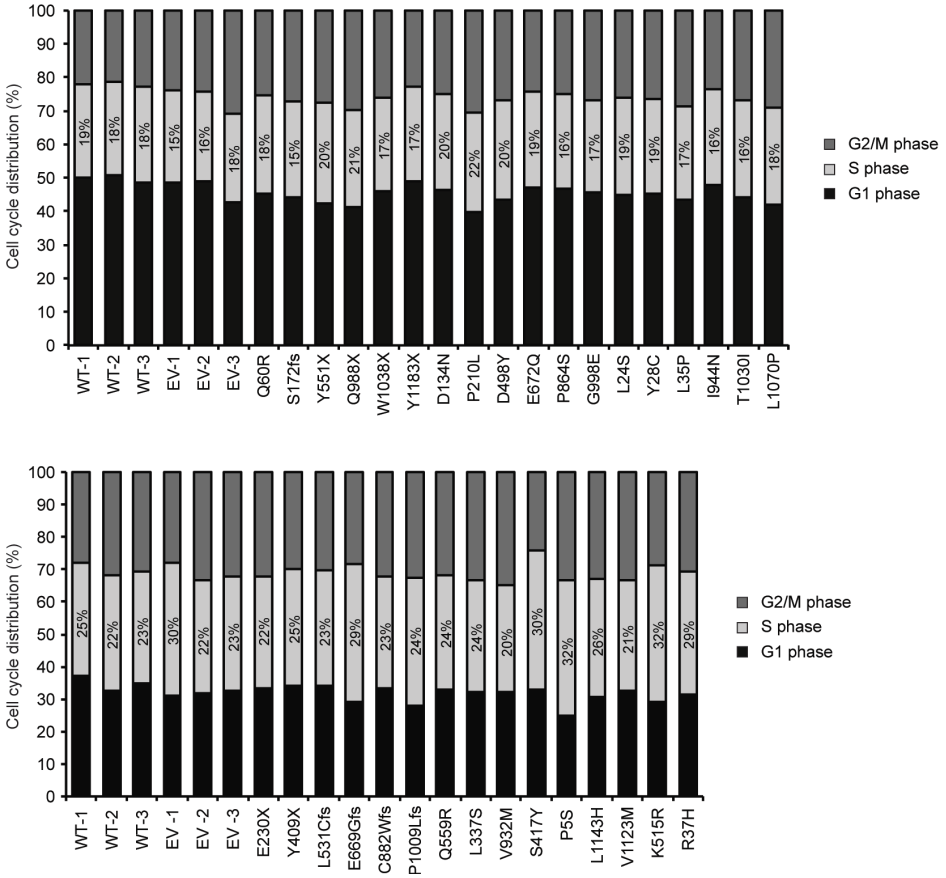

Supplementary Figure 8. Cell cycle profiles of *Trp53*^{KO}/*Palb2*^{KO} mES cells expressing human *PALB2* variants. Cell cycle profiles are from cells in Fig. 2b. Cells were treated with propidium staining (PI) and analyzed by FACS. Data represent the mean percentage of cell cycle phase distributions from 2 independent measurements. Source data are provided as a Source Data file.

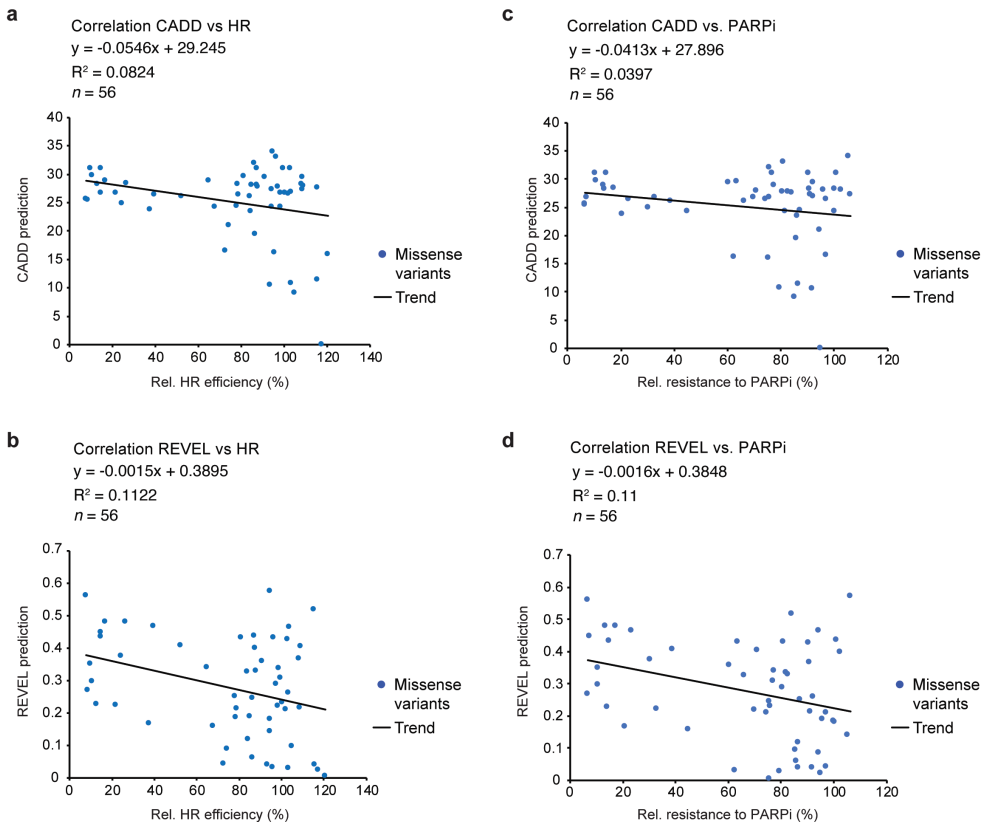

Supplementary Figure 9. Correlation between *in silico* predictions and the outcome of functional assays for missense variants in human *PALB2*. **a** Scatter plot showing correlation between the *in silico* prediction from CADD and results from the DR-GFP assay in Fig. 2b. **b** Scatter plot showing correlation between the *in silico* prediction from REVEL and results from the DR-GFP assay in Fig. 2b. **c** Scatter plot showing correlation between the *in silico* prediction from CADD and results from the PARPi sensitivity assay in Fig. 3a. **d** Scatter plot showing correlation between the *in silico* prediction from REVEL and results from the PARPi sensitivity assay in Fig. 3a.

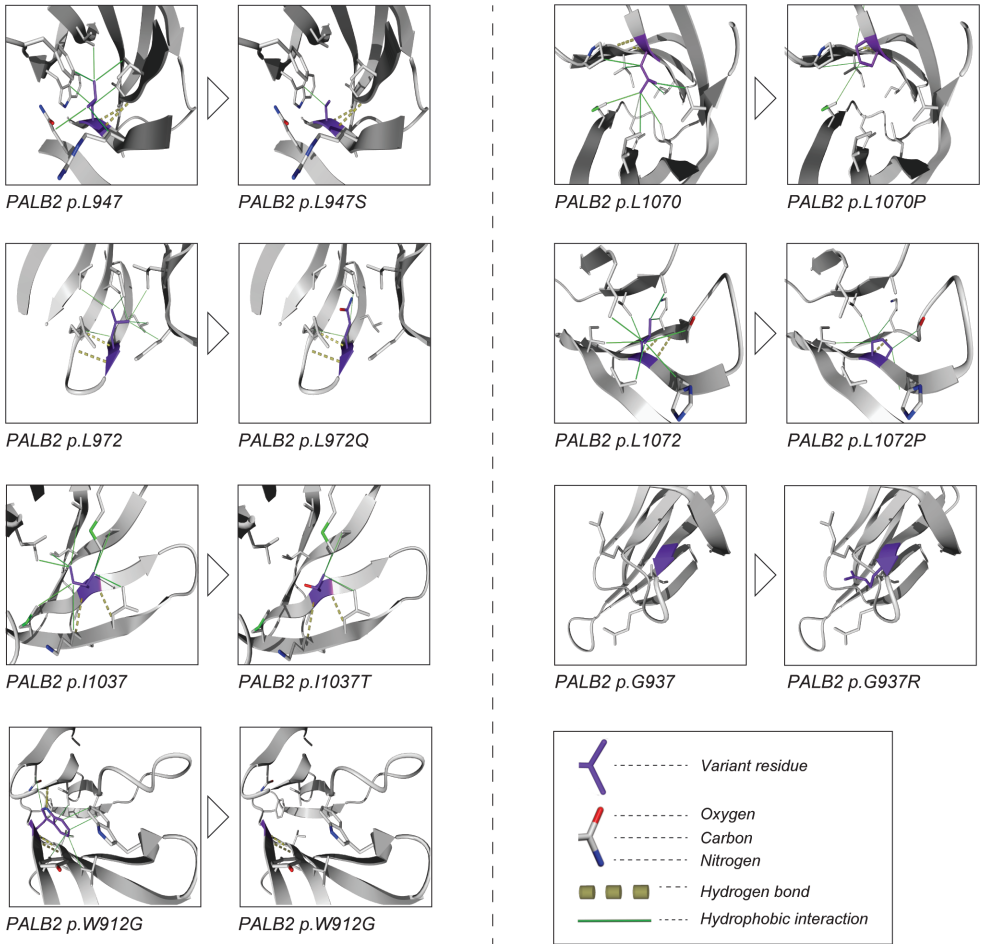

Supplementary Figure 10. Effect of *PALB2* variants on protein stability. Partial structures of the PALB2 WD40 domain showing the effect of 7 PALB2 variants exhibiting low protein expression as shown in Fig. 4a. Partial structures without and with variant are shown side by side for each variant, indicating loss of stabilizing interactions (but not any possible conformational changes).

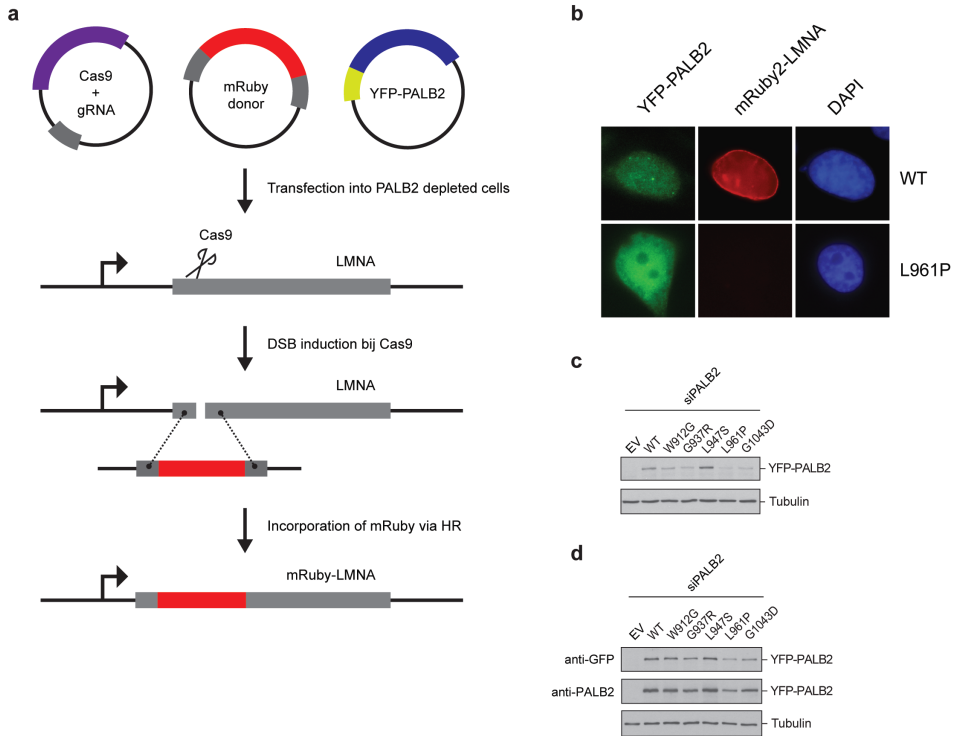

Supplementary Figure 11. Functional analysis of damaging *PALB2* variants in human cells. **a** Schematic of the CRISPR-LMNA HDR assay in human cells. Homology-directed repair of the Cas9-induced DSB will result in the in-frame integration of mRuby in the first exon of *LMNA*, leading to expression of red fluorescent mRuby-LMNA. The number of mRuby-positive cells is a measure of the HR efficiency. **b** Representative fluorescence microscopy images of mRuby2-LMNA expression after successful homology directed repair (HDR) in a PALB2-depleted U2OS cell complemented with YFP-PALB2-WT (upper), and a cell negative for mRuby2-LMNA expression after complementation with the damaging YFP-PALB2-L961P variant (lower). **c** Western blot analysis of the expression of human PALB2 variants in si*PALB2*-treated U2OS cells 24 hours after complementation with the indicated siRNA-resistant YFP-*PALB2* variant cDNA constructs. Tubulin was used as a loading control. **d** Western blot analysis of the expression of human PALB2 variants in si*PALB2*-treated HeLa cells 24 hours after complementation with the indicated siRNA-resistant *YFP-PALB2* variant cDNA constructs. Tubulin was used as a loading control. Source data are provided as a Source Data file.